Mon. Not. R. Astron. Soc. **328,** 527–554 (2001)

SwSt 1: an O-rich planetary nebula around a C-rich central star

Orsola De Marco,[1,2,3★] P. A. Crowther,[3] M. J. Barlow,[3] Geoffrey C. Clayton[2] and A. de Koter[4]

[1]*Department of Astrophysics, American Museum of Natural History, Central Park West at 79th Street, New York, NY 10024, USA*
[2]*Department of Physics and Astronomy, Louisiana State University, Baton Rouge, LA 70803, USA*
[3]*Department of Physics and Astronomy, University College London, Gower Street, London WC1E 6BT*
[4]*Astronomical Institute 'Anton Pannekoek', University of Amsterdam, Kruislaan 403, 1098 Amsterdam, the Netherlands*

Accepted 2001 August 6. Received 2001 August 1; in original form 2001 March 13

ABSTRACT

The hydrogen-deficient [WCL] type central star HD 167362 and its planetary nebula (PN) SwSt 1 are investigated. The central star has a carbon-rich emission-line spectrum, and yet the nebula exhibits a 10-μm emission feature from warm silicate dust, perhaps indicating a recent origin for the carbon-rich stellar spectrum. Its stellar and nebular properties might therefore provide further understanding as to the origin of the [WCL] central star class.

The central star optical and UV spectra are modelled with state-of-the art non-LTE codes for expanding atmospheres, from which the stellar parameters are determined. Using the Sobolev approximation code ISA-Wind, we find $T_{\rm eff} = 40000$ K, $\log(\dot{M}/{\rm M}_\odot\,{\rm yr}^{-1}) = -6.72$, $L = 8900\,{\rm L}_\odot$ (for a distance of 2.0 kpc), and $v_\infty \simeq 900\,{\rm km\,s}^{-1}$. The abundance mass fractions for helium, carbon and oxygen are determined to be 37, 51 and 12 per cent, respectively. From this we derive C/O $= 4.3$ (by mass), confirming that the star suffered efficient third dredge-up. The nitrogen abundance is close to zero, while an upper limit of <10 per cent by mass is established for H. The model uses a composite beta velocity law which allows us to reproduce the optical line profiles. The overall shape of the dereddened spectrum agrees with the *V*-scaled [$m_V = 11.48$ mag, $E(B-V) = 0.46$ mag] model atmosphere, showing the nebular-derived reddening to be consistent with the reddening indicated by the stellar analysis. We confirm our model results by using the comoving frame code CMFGEN, although a few differences remain.

The PN has a high electron density [$\log(N_{\rm e}/{\rm cm}^{-3}) = 4.5$] and a small ionized radius (0.65 arcsec – measured from the *HST*-WFPC Hβ images), indicating a young object. Its nebular abundances are not peculiar. The nebular C/O ratio is close to solar, confirming the PN as an O-rich nebula. The nebular N/O ratio of 0.08 is *not* indicative of a Type-I PN, although the high stellar luminosity points to a relatively high stellar mass. Near-IR spectroscopy is presented and fitted together with *IRAS* fluxes by using two blackbody curves with temperatures of 1200 and 230 K, indicating the presence of hot dust. We also report the first detection of H_2 in this young and compact PN.

All of the published spectroscopy since the discovery of SwSt 1 in 1895 has been re-examined, and it is concluded that no clear spectral variability is seen, in contrast to claims in some previously published studies. If an event occurred that has turned it into a hydrogen-deficient central star, it did not happen in the last 100 years.

Key words: stars: abundances – stars: AGB and post-AGB – stars: atmospheres – stars: evolution – stars: Wolf–Rayet – planetary nebulae: individual: SwSt 1.

★E-mail: orsola@amnh.org

1 INTRODUCTION

[WCL][1] central stars of planetary nebulae (PNe) are hydrogen-deficient central stars that exhibit emission-line spectra very similar to massive Wolf–Rayet stars. Until recently it has been impossible to calculate stellar evolutionary models where the star eliminates all of its hydrogen-rich envelop at the top of the asymptotic giant branch (AGB). This prompted the association of these objects with the born-again scenario (Iben et al. 1983), whereby a white dwarf experiences a last helium shell flash, after which it rejoins the tip of the AGB for a second time and repeats its evolution, this time as a hydrogen-deficient central star.

The PNe around [WC] central stars do not appear to have any characteristics which distinguish them from the PNe of hydrogen-rich central stars. A marginally higher nebular C/H ratio (De Marco & Barlow 2001), as well as a slightly higher PN expansion velocity (Gorny & Stasinska 1995), do not appear to be sufficient to characterize the evolution of the sample. Other puzzling peculiarities concern spectral appearance differences amongst members of the hydrogen-deficient central star group. Some hydrogen deficient central stars appear to have weaker lines than others [called *weak emission-line stars* (*wels*) by Tylenda, Acker & Stenholm 1993], while in the strong-lined [WC] group there appears to be a classification gap, with [WC] stars populating the [WC11-8] class (called [WCL]) and [WC5-WO1] (called [WCE]; Pottasch 1996; Crowther, De Marco & Barlow 1998). Additionally, while it is currently believed that [WCL] stars evolve into [WCE] stars, the stellar abundances seem to differ in the two groups, with the more evolved group having a lower carbon abundance than the less evolved group (see De Marco & Barlow 2001 for a summary of results from the literature), a fact that cannot be easily explained.

On the other hand, *Infrared Space Observatory* (*ISO*) spectroscopy of PNe with [WCL] central stars has shown that all have crystalline silicate features in their mid- to far-infrared spectra, in addition to the previously known carbon-rich PAH-type features that dominate their mid-infrared spectra, betraying the simultaneous presence of both carbon-rich and oxygen-rich dust (see Barlow 1997; Waters et al. 1998, Cohen et al. 1999 and Cohen 2001). The relatively warm temperatures deduced for the O-rich dust, together with the high nebular densities of their compact nebulae, appear to imply that the C-rich central stars evolved relatively recently from an O-rich composition. This would in turn suggest that these [WCL] PNe have been on the AGB recently, and so did not result from a born-again evolutionary phase, for which low-density nebulae are expected. This would also imply that the carbon-rich [WCL] stars systematically result from oxygen-rich AGB giants.

Recent improvements in theoretical stellar evolutionary calculations have succeeded in eliminating hydrogen from the stellar atmosphere at the tip of the AGB, so that the requirement that the central star undergo a born-again event in order to get rid of its hydrogen is no longer in place. According to Herwig (2000) a thermal pulse just before the star departs from the AGB can eliminate most of the hydrogen, while a well-timed post-AGB pulse (probabilistically rarer) could account for the extreme hydrogen deficiency observed in [WCL] stars. The combination of the *ISO* observations and the new evolutionary calculations therefore contributes to the revision of theories about the origin of [WCL] central stars, and for the first time we may have a viable scenario that does not require the star to go through a born-again episode.

The PN SwSt 1 around the central star HD 167362 (we will give both star and nebula the name SwSt 1) exhibits a broad 10-μm silicate emission feature (Aitken & Roche 1982) and has been suggested to be amongst the youngest of [WCL] nebulae, possibly having experienced the transition from the AGB in the last century. The spectrum of SwSt 1 was first reported by Fleming (1895), but the first complete spectroscopic analysis was carried out by Swings & Struve (1940, 1943). The traditional WR C IV λ5806/C III λ5696 line diagnostic ratio positions it within the [WC9] spectral class (Crowther et al. 1998 – see also previous classifications by Cohen 1975 and by Carlson & Henize 1979), but the weakness of its lines compared to other [WC9] stars (e.g., BD + 30°3639, He 2-99) or even cooler [WC10] stars (e.g., CPD − 56°8032, He 2-113, M 4-18) prompted Crowther et al. (1998) to flag it as *peculiar*, and has therefore essentially left it in a class of its own. Tylenda et al. (1993) listed it amongst their *wels* because of the weakness of its spectral lines, but SwSt 1 does not resemble stars in this class either (e.g., Cn 3-1; De Marco et al. 2000) since it has many more stellar emission features than any *wels*, indicative of a denser wind.

In this paper we tried to determine whether the physical characteristics of the central star and the PN can shed light on the reason for these differences, i.e., whether SwSt 1 is at an intermediate phase between stars in the [WCL] class and their ancestors. In the sections that follow we present optical echelle spectra, near-infrared spectra and archival *IUE* spectra, as well as *HST* images of this central star and its PN. Using these data, we carry out a thorough analysis, to try and single out the peculiarities of this object. In Section 2 we present our observational data, while in Section 3 we derive some observational parameters. The distance, luminosity and mass are discussed in Section 4. The stellar analysis is tackled in Section 5, while the nebular analysis is carried out in Sections 6 to 8. Finally (Section 9), a review of the secular variability is reported, and conclusions are drawn in Section 10.

2 OBSERVATIONS

SwSt 1 was observed with the 3.9-m Anglo-Australian Telescope (AAT) on 1993 May 14 and 15, using the 31.6 line mm^{-1} grating of the UCL Echelle Spectrograph (UCLES), with a 1024×1024 pixel Tektronix CCD as detector. Four settings of the CCD were needed in order to obtain spectral coverage in the range 3600–9700 Å. At each wavelength setting, 5-arcsec wide-slit spectra were obtained for absolute spectrophotometry, while 1.5-arcsec narrow-slit spectra ($R = 50\,000$) were obtained for maximum resolution in the range 4100–5400 Å. The continuum signal-to-noise ratio of the averaged exposures ranges from ∼5 in the far blue to ∼30 in the red. A log of the observations is presented in Table 1.

The data were reduced using the IRAF (V2.10)[2] package at the UCL Starlink node. Wavelength calibration was with respect to comparison Th-Ar arc exposures. Absolute flux calibration was with respect to the B3IV star HD 60753, whose energy distribution has been measured by Oke (1990). Details of the laborious echelle data flux-calibration procedure can be found in De Marco, Barlow & Storey (1997, hereafter DBS97). Subsequent data reduction was

[1] 'WC' stands for Wolf–Rayet of the carbon sequence, and 'L' stands for 'late' as opposed to the hotter members of this class, the [WCE]. The brackets were introduced by van der Hucht et al. (1981) to differentiate Wolf–Rayet central stars from massive central stars.

[2] IRAF is written and supported by the National Optical Astronomy Observatories (NOAO) in Tucson, Arizona; http://iraf.noao.edu/

Table 1. Log of the 1993 UCLES observations of SwSt 1. Only the second night was photometric.

Central λ (Å)	Date 1993 May	Exp. Time (s)	Slit Width (arcsec)	Airmass	Seeing (arcsec)
4622	14	2×900	1.5	1.2	3
4622	14	300	5.0	1.14	2.5
6827	15	900	5.0	1.6	2
6960	15	600	5.0	1.5	2
4622	15	300	5.0	1.4	2
3712	15	500	5.0	1.4	2
6827	15	60	5.0	1.3	2
6960	15	60	5.0	1.3	2

Table 2. Radial and expansion velocities (Columns 1 and 2) for SwSt 1 obtained from the Balmer emission lines. Radial velocities for the Na I D absorption line components are also presented (Column 3). Finally, distances derived from two different methods are presented in Columns 4 and 5.

LSR RV ($km\,s^{-1}$)	PN Expansion Velocity ($km\,s^{-1}$)	LSR RV of Na I ($km\,s^{-1}$)	D^a (kpc)	D^b (kpc)
-8.1 ± 1.0	21 ± 2	$-78, -38, +8$	4.9	3.0

[a]Distance derived from Na I D positive line components.
[b]Distance derived from the IR flux method.

carried out with the Starlink DIPSO package (Howarth et al. 1995). After flux calibration, the narrow-slit spectra were scaled up to the continuum level of the wide−slit spectra.

International Ultraviolet Explorer (*IUE*) observations of SwSt 1 were also used. The retrieved LWR and SWP spectra were divided up according to the aperture used for their acquisition, and the weighted average was used. One SWP observation (SWP17068) was taken in high-resolution mode and, although its signal-to-noise ratio was rather poor, it could be used for parts of our analysis.

2.1 Near-IR spectroscopy: first detection of H_2 in a young WCL-type central star

Long-slit, near-IR spectroscopy of SwSt 1 was acquired on 1999 September 1 with the NTT, using the Son OF Isaac (SOFI) instrument, a 1024×1024 pixel NICMOS detector, and low-resolution IJ (GRB) and HK (GRR) gratings. The spectral coverage was 0.94–1.65 and 1.50–2.54 μm, respectively, with dispersions of 7.0 and 10.2 Å $pixel^{-1}$. The 0.6-arcsec slit provided a two-pixel spectral resolution of 14–20 Å. The total integration time was 480 s at each grating setting. The removal of atmospheric features was achieved by observing HD 169101 (A0V) immediately before and after SwSt 1, at a close airmass (within 0.03). Similar observations of HD 166733 (F8) permitted a relative flux correction, using a $T = 6100$ K model atmosphere normalized to $V = 9.59$ mag.

A standard extraction and wavelength calibration was carried out with IRAF, while FIGARO (Shortridge et al. 1999) and DIPSO (Howarth et al. 1995) were used for the atmospheric and flux calibration, first artificially removing stellar hydrogen features from the B3V spectrum. Our relatively fluxed data set was adjusted to match previously published near-IR photometry (Allen & Glass 1974) via convolution with the appropriate filter profiles. The spectrum is presented in Appendix B.

We can also report on the first detection of H_2, at 2.1218 μm [$v = 1$–0, S(1)] from this young, late WC-type central star PN system. Although the presence of H_2 is well established in slightly more evolved [WC] systems such as the [WC9] PN BD + 30°3639 (Kastner et al. 1996), it has not been detected from some young, high-density PNe with bright central stars, e.g., IC 4997 and 418 (Zuckerman & Gatley 1988; Kastner et al. 1996). This appears to be due to their strong H_2-dissociating UV radiation fields. The relative weakness of SwSt 1's H_2 emission may indicate that the neutral regions surrounding this nebula are also mainly atomic rather than molecular. This is in agreement with the fact that no CO is detected in the neutral envelope of SwSt 1 (Huggins et al. 1996).

3 OBSERVATIONAL QUANTITIES

3.1 Apparent magnitudes

We convolved our observed central star wide-slit spectrophotometry of SwSt 1 with broad-band V and B filter profiles (kindly made available to us by Dr J. R. Deacon) to obtain an estimate of the apparent V and B magnitudes of the stars. We derive $V = 11.48$ mag, and $B = 11.54$ mag. Convolving with narrow-band (Smith 1968) filter profiles, we derive $v = 11.69$ mag and $b = 11.73$ mag. The *Hipparcos* and Tycho catalogues quote a Johnson V magnitude of 10.94 mag, Hpmag = 10.86 mag (median magnitude in *Hipparcos* system) and an observed Hp range of 10.79–10.97 mag. However, SwSt 1 is near the faint limit of the Tycho detector of ∼12 mag. The visual photometry of A. Jones reveals a mean magnitude of (10.4 ± 0.5) mag, with no sign of variability (Jones et al. 1999).

We finally decided to adopt our own spectro-photometric values, since our spectrophotometry aligns perfectly with *IUE and* near-IR SOFI data and since broad-band photometry of emission-line central stars can be contaminated by stellar and nebular emission-line fluxes. Although the visual photometry of Jones et al. (1999) shows the lack of intrinsic stellar variability, photometry of SwSt 1 carried out by A. Landolt (private communication) on 2001 February 19, 20 and 23 indicates $V = 11.57$ mag (in the standard system of Landolt 1992),[3] slightly fainter than our own spectrophotometry as well as all the other estimates, and indicating that variability might be present.

3.2 Nebular radial and expansion velocities

Nebular radial velocities were obtained by determining the average wavelength shift of the nebular Balmer lines using a single Gaussian fit. Even when a single Gaussian did not fit the data very well, it was felt that this would be the best way to locate the overall centre of the line without biases introduced by asymmetry. The heliocentric radial velocity was measured to be $(-17.8 \pm 1.0)\,km\,s^{-1}$ from an average of the Hβ, Hγ and Hδ lines; the LSR radial velocity was determined to be $(-8.1 \pm 1.0)\,km\,s^{-1}$. These estimates compare well with those of Schneider et al. (1983; $V_{LSR} = -8.7\,km\,s^{-1}$, $V_{Helio} = -18.6\,km\,s^{-1}$). Radial velocities are listed in Table 2, together with nebular expansion velocities

[3] This is the average of six estimates, two per night in the range 11.55–11.59 mag. The aperture used was 14 arcsec wide. Two or three faint stars were included in the aperture, such that this estimate might be slightly too high, yet it is fainter than anything reported before. From the same photometry the following colours are reported: $B - V = +0.078$, $U - B = -0.960$, $V - R = +1.283$, and $R - I = -0.498$.

measured from averaging the HWHM of $H\beta$, Hγ and Hδ (Hα was saturated).

3.3 Reddening

The reddening was derived by comparing the relative fluxes in the nebular Hβ, Hγ and Hδ lines (Hα was saturated). Using the Case B hydrogen recombination coefficients of Storey & Hummer (1995) for a nebula with electron density $N_e = 10^4\,cm^{-3}$ and $T_e = 10^4\,K$ and the Galactic reddening law of Howarth (1983), values of $E(B-V)$ were derived. The reddening was also derived from a comparison of the radio and Hβ fluxes, using the method of Milne & Aller (1975). In Table 3 we list Balmer line fluxes measured from wide-slit AAT spectroscopy, together with fluxes from the literature. Considerable discrepancies exist between the Hβ flux measured here and measurements found in the literature. From Table 3 we see that our own value is about one-third higher than most of the other values, although Acker, Stenholm & Tylenda (1989) measured an even higher Hβ flux. The possibility of a true variation in time was therefore investigated, but no clear trend exists in either the Hβ fluxes or in the radio flux measurements. Although these large differences remain suspicious, we must attribute them to calibration and measurement errors, and possibly to some slit/aperture widths not including all of the PN.

Table 3. Wide-slit (5 arcsec) fluxes (erg cm^{-2} s^{-1}) measured for the nebular hydrogen lines of SwSt 1, compared with values from the literature.

Reference	Hβ	Hγ	Hδ
AAT (1993)	3.19×10^{-11}	1.20×10^{-11}	6.53×10^{-12}
Perek (1971)	1.66×10^{-11}	–	–
FGC84	2.14×10^{-11}	7.24×10^{-12}	–
dFV87	1.82×10^{-11}	–	–
AST89	5.89×10^{-11}	–	–

FGC84 = Flower, Goharji & Cohen 1984
dFV87 = de Freitas Pacheco & Veliz 1987
AST89 = Acker, Stenholm & Tylenda 1989

Table 4. Reddenings derived from Balmer line ratios and from the radio–Hβ baseline for SwSt 1.

Ratio	$E(B-V)$ AAT (1993)	$E(B-V)$ FGC84	$E(B-V)$ dFP87	$E(B-V)$ P71
Hα/Hβ	–	–	–	–
Hβ/Hγ	0.51[a]	–	–	–
Hβ/Hδ	0.41[a]	–	–	–
radio/Hβ	0.30	0.34	0.41	0.50[b]

FGC84 = Flower, Goharji & Cohen 1984.
GD85 = Goodrich & Dahari 1985.
dFV87 = de Freitas Pacheco & Veliz 1987.
P71 = Perek 1971.
[a] We adopted 0.46, the average of 0.51 and 0.41.
[b] Derived by us using his Hβ flux.

In Table 4 we list our results, together with reddenings selected from the literature for comparison. From the Hβ–Hγ baseline in our UCLES wide-slit (5-arcsec) spectrum, we determine $E(B-V) = 0.51$, while from the Hβ–Hδ baseline we find $E(B-V) = 0.41$. Radio fluxes at 15 GHz have been measured by Kwok et al. (1981; 207 ± 11 mJy), Milne & Aller (1982; 240 ± 12 mJy) and Aaquist & Kwok (1990; 175 ± 17 mJy). The weighted average (211 ± 17 mJy) corresponds to a 5-GHz flux of 243.0 mJy for optically thin free–free emission, which we adopted, together with our UCLES value for the Hβ flux, to derive $E(B-V) = 0.30$. A similar value is also obtained by nullying the 2200-Å feature. Comparison of the Perek (1971) photoelectric flux with the mean radio flux yields $E(B-V) = 0.50$.

We adopt $E(B-V) = 0.46 \pm 0.05$, the mean obtained from the Hβ/Hγ and Hβ/Hδ ratios, as the most self-consistent estimate we have. Pre-emptying the results of Section 5.5, the slope of the synthetic stellar atmosphere model carried out with the ISA-Wind code, which fits the stellar emission-line intensities, agrees with the nebular line reddening estimate of $E(B-V) = 0.46$. For the model carried out with the CMFGEN code, the best match is obtained with $E(B-V) = 0.48$. These values are also in reasonable agreement with the determination of $E(B-V) = 0.50$ quoted above, from the radio and the photoelectric Hβ fluxes.

Finally, the near-IR spectrum is dominated by strong nebular emission lines of H I (e.g., Pβ, Brγ) and can be used to obtain a further confirmation of the reddening. For $E(B-V) = 0.46$ and the nebular properties derived in Section 6, agreement with Case B recombination theory (Storey & Hummer 1995) is very good. For instance, $I(P\beta)/I(H\beta) = 0.16$ (0.15 from Case B), or $I(Br\gamma)/I(H\beta) = 0.024$ (0.024 from Case B). Pα is an exception, but this lies in a region of poor atmospheric transmission.

4 LUMINOSITY AND DISTANCE

In Table 5 we summarize the distances that have been determined for SwSt 1 in the literature, together with our two estimates from

Table 5. Summary of the distances determined for SwSt 1 in the literature using various methods.

Distance (kpc)	Method	Reference
1.0	extinction method	de Freitas Pacheco & Veliz 1987
1.1	modified Shklowskii	de Freitas Pacheco & Veliz 1987
>1.2	*Hipparcos*	Acker et al. 1998
1.4	Shklowskii	Cahn et al. 1992
1.4	M_v–T_* relationship	de Freitas Pacheco & Veliz 1987
3.0	LMC [WC] star calibration	this work
3.1	M and gravity	Zhang 1993
3.2	$I(H\beta)$ for opt. thick PN[a]	Kingsburgh & Barlow 1992
3.8	ionized mass – R(PN) and radio Tb–R(PN) corr	Zhang 1995
4.7	radio cont. brightness and R(PN)	van de Steene & Zijlstra 1994
4.9	Galactic rotation curve	this work
5.0	L_*	Zhang 1993

[a]We used their equation (11) and our $\log[I(H\beta)] = -10.1$ from Section 8.1.

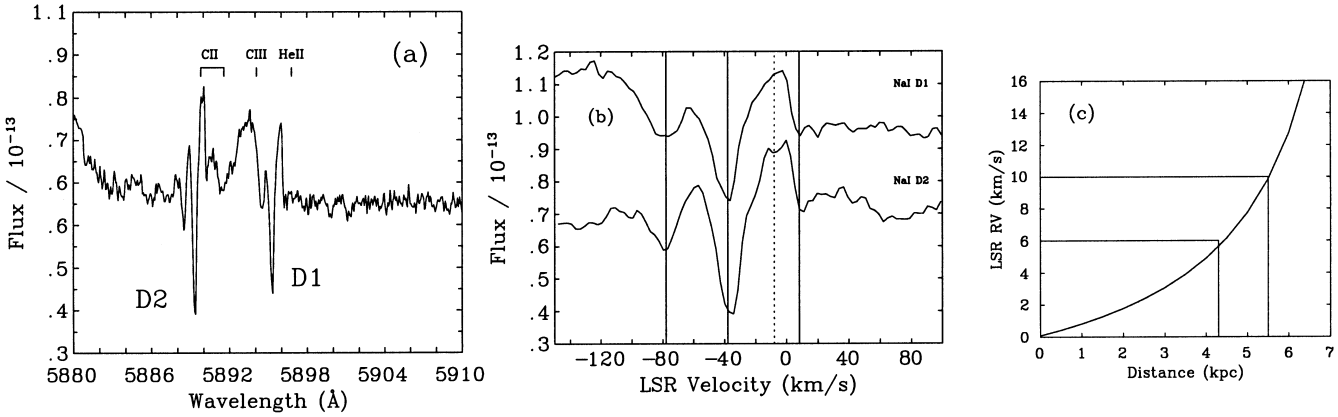

Figure 1. (a) The Na I D lines towards SwSt 1 (where the wavelength scale has been corrected for a heliocentric radial velocity of $-17.8\,\mathrm{km\,s^{-1}}$ and where we have indicated the positions of C II Multiplet 5, C III Multiplet 20 and the He II λ5896.8 line. (b) The Na I D lines displayed in their LSR rest frame. The D2 line has its original flux units, while the D1 line has been displaced upwards by an additive factor of 3×10^{-14}. The dotted line marks the LSR radial velocity of the nebula, while the solid lines show the positions of the three most prominent Na I absorption components. (c) The Galactic rotation curve for the direction of SwSt 1. The distances corresponding to LSR radial velocities of +6 and $+10\,\mathrm{km\,s^{-1}}$ are 4.3 and 5.5 kpc.

Sections 4.1 and 4.2. Below we explain our two methods, but admit that there is no convincing estimate for the distance to SwSt 1 beside the fact that after iterating between an assumed distance and our models we have gained further insight which restricts the range of possible distances (see Sections 5 and 6), leading us to finally adopt a distance of 2.0 kpc (Section 4.3).

4.1 Distance from a Magellanic Cloud luminosity calibration

DBS97 used Magellanic Cloud Wolf–Rayet central stars to derive a mean central star mass for WC central stars of $0.62\,\mathrm{M_\odot}$. This mass was then applied together with the helium-burning tracks of Vassiliadis & Wood (1994) to derive luminosities for CPD −56°8032 and He 2–113 corresponding to their effective temperatures, which were in turn used, together with their integrated IR fluxes, to determine their distances. The PN of SwSt 1, with a high electron density, a small apparent radius and a significant IR excess, appears to be a good candidate to apply the same method. We have obtained from the *ISO* archive the SWS01 spectrum of SwSt 1 (from the program of S. K. Gorny, TDT47101511, reduced with SWS OLP Version 9.5; Szczerba et al. 2001). This spectrum is plotted in Fig. 6, together with its photometric fluxes at 1.65 and 2.2 μm (Allen & Glass 1974) and colour-corrected *IRAS* fluxes. Integration under the IR spectrum of SwSt 1 between 1.6 and 100 μm results in a flux of $1.48 \times 10^{-8}\,\mathrm{erg\,s^{-1}\,cm^{-2}}$, corresponding to an infrared bolometric luminosity of $463\,D^2(\mathrm{kpc})\,\mathrm{L_\odot}$. For $T_{\rm eff} \sim 40\,000$ K (Section 5), the helium-burning tracks of Vassiliadis & Wood (1994) predict a luminosity of $4280\,\mathrm{L_\odot}$, where we interpolated between the tracks for 0.600-$\mathrm{M_\odot}$ and 0.634-$\mathrm{M_\odot}$ cores. The distance obtained in this way is 3.0 kpc (a $T_{\rm eff} \sim 35000$ K predicts $4670\,\mathrm{L_\odot}$ and a distance of 3.2 kpc).

The three key assumptions of this method are (a) SwSt 1 has the same mass as the LMC [WC] stars, (b) all its luminosity is re radiated in the IR by dust, and (c) the helium-burning track calculations are valid. By far the most compromising assumption is that all [WC] stars have the same mass (as suggested by De Marco & Crowther 1999, this is likely not to be the case). We have therefore determined the distances corresponding to all three masses calculated by Vassiliadis & Wood (1994), namely 0.57, 0.60 and $0.63\,\mathrm{M_\odot}$. These are 2.1, 2.5 and 3.6 kpc, respectively. We therefore conclude that if assumptions (b) and (c) hold, the distance is in the range ∼2.0–3.5 kpc.

4.2 Galactic rotation curve distance

In order to obtain an alternative value for the distance, we applied the interstellar sodium D line method used by DBS97. In Fig. 1(a) we show the spectral range containing the Na I D lines, while in Fig. 1(b) we show Na I D1 and D2 lines in their respective LSR rest frames. From Figs 1(b) and (c) we see that the line of sight to SwSt 1 has a positive rotation curve, while most of the Na I D line components have negative radial shifts. The only interstellar component with positive velocity is measured at $(+8 \pm 2)\,\mathrm{km\,s^{-1}}$ (see Fig. 1b) and corresponds to a distance of (4.9 ± 0.6) kpc, where the uncertainty derives solely from locating the centre of the trough. The underlying stellar emission lines (C II λλ5889,92, C III λ5894 and He II λ5897) are too weak to achieve a reliable rectification, which would lead to an increase in the measurement precision. Moreover, the Na I D lines have emission components (as noticed by Dinerstein, Sneden & Uglum 1995) and a multiple cloud fit would over-interpret the data, so we limited ourselves to measuring the centres of the absorption components. The negative radial velocity troughs are likely to derive from the PN's neutral envelope, and are discussed in Appendix A.

4.3 The adopted distance

Although each method listed in Table 5 has its limitations and it is beyond the scope of this paper to review each of the different estimates, we should note that two of the best methods to estimate distances to Galactic objects suffer from additional caveats. SwSt 1 is too far for the *Hipparcos* distance, derived from a parallax of (8.9 ± 6.0) mas (HIP89535; Acker et al. 1998), to be considered reliable. Second, the extinction distance is based on the assumption that within 2 kpc of the Sun, light suffers 0.4 mag of extinction per kpc, and is not based on an extinction map, which would make the method more reliable.

Although our estimates seem to point to a fairly large distance (i.e., ∼3–5 kpc), we found in our modelling of the stellar spectrum that a very high luminosity and central star mass were implied by a distance larger than 2 kpc, and would have required the central star

to have evolved significantly in effective temperature in the last 100 years. Such evolution would have been mirrored by significant spectral changes. This, however, has not been observed (see Section 9). We therefore adopt 2 kpc as the distance to SwSt 1, but admit a substantial uncertainty.

5 STELLAR ANALYSIS

In this section we carry out a stellar atmosphere analysis of SwSt 1 to derive the stellar effective temperature and mass-loss rate as well as its carbon and oxygen abundances. The line-blanketed stellar flux resulting from this analysis is then used as input for the photoionization model of the PN (Section 8).

5.1 The near-IR, optical and UV stellar spectra

The spectrum of SwSt 1 contains a mixture of stellar and nebular emission lines. The stellar lines are weaker and fewer than for the [WC10] central stars CPD −5680°8032 and He 2-113 (DBS97), while the nebular lines are stronger. The nebular Balmer lines, the lines of He I, and, to a lesser extent, those of C II and O II, could be blends of stellar and nebular emission. In particular, the UV C III] λ1909 is a blend of stellar and nebular emission, with the nebular emission contributing about 40 per cent of the flux to this feature (Fig. 7). The C II] λ2326 feature is thought to be mostly of nebular origin, although this cannot be checked since only low-resolution *IUE* data exist for this wavelength range. The UV C III–IV and Si IV emission lines are entirely of stellar origin.

In Section 5.1.1 we will show that it is unlikely that hydrogen is present in the star, so that the main contributors to the Balmer lines are likely to be nebular hydrogen and, to a much lesser extent, stellar He II. Additionally, there is no evidence of a significant stellar contribution to the strong nebular He I lines. Except for λ5876, which exhibits a broad pedestal at the base of the nebular component, other strong He I lines at 3889, 4471, 4713 and 6678 Å show no evidence of having a stellar component. The broad pedestal at the base of He I λ5876 is likely to belong in part to C III M 20, with components at (in order of intensity) 5894.07, 5871.69, 5858.35, 5880.54, 5863.24 and 5872.10 Å, since the four strongest components are observed at approximately the predicted relative strengths. In the near-IR we observe He I at 1.083 μm, although the lower resolution of this spectrum does not allow us to distinguish between nebular and stellar components to this line. Stellar He II λ4686 is clearly visible in emission; He II λ5411 has a weak P Cygni absorption, but its emission, if present, is blended with the nebular [Fe III] line at 5412.0 Å; He II λ4541 has a weak emission to a blueshifted absorption.

C III lines dominate over C II lines in SwSt 1's spectrum, indicating a higher degree of ionization than for the two [WC10] stars analysed by DBS97. In the optical we observe C III λ4650, λ5696, λ8500. λ8500 is a blend of three lines: the stellar C III λ8500, a strong nebular line with radial velocity-corrected wavelength at 8502.1 Å, likely to be itself a blend of H I Paschen 16 and [Cl III] λ8500 ([Cl III] λ8481 is also present), and a weaker line at 8499.7 Å. An unidentified nebular line at this spectral position was also observed by Keyes, Aller & Feibelman (1990) in the spectrum of NGC 7027. In the near-IR SOFI spectrum we observe C III at 9710 Å, and at 1.198 μm.

C IV λλ5801,12, λ5470 and λ4441 are observed, albeit weakly, while in the UV we see C IV λλ1548,1551. C II lines are observed at 4267, 6578 and 7231.3 Å (blended with telluric absorptions). All C II features exhibit stellar as well as nebular components.

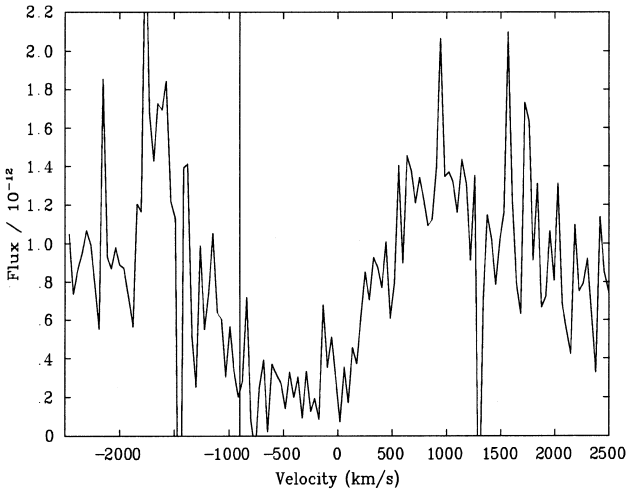

Figure 2. The C IV resonance doublet profile in the high-resolution *IUE* spectrum (SWP17068HL). The *x*-axis has been converted to velocity space; $v = 0\,\mathrm{km\,s^{-1}}$ corresponds to 1548.2 Å, the bluer of the two components of the doublet (at 1548.2 and 1550.8 Å). The vertical line marks the chosen $v_{\mathrm{black}} = -900\,\mathrm{km\,s^{-1}}$.

Semiforbidden C II] λλ2324.2,2325.4 (likely to be entirely of nebular origin) and C III] λλ1906.7,1908.7 (having a nebular as well as a stellar component – Fig. 7) are also observed.

O III λ5592 is observed in emission with a weak P Cygni absorption, while the O II stellar spectrum is very weak (e.g., λλ4591.0,4596.0). No nitrogen lines are observed, although there is a possibility that a feature observed in the high-resolution *IUE* spectrum at 1718.92 Å is indeed N IV λ1718.5 and not Si IV λ1722.5. The optical lines of nitrogen used by Leuenhagen & Hamann (1998) (i.e., N III λλ4097,4104) to determine an upper limit for the abundance of nitrogen are not observed in our spectrum. N II λ3995 and λ4682 are also unobserved. The N V line marked by Flower et al. (1984) in the UV spectrum at 1438.8 and 1442.8 Å is almost certainly C III λ1347.4. Si IV λλ1393.7,1402.8 are observed in the UV spectrum, as are weak optical lines at 4089 and 4116 Å (M1).

From the high-resolution *IUE* spectrum of the C IV λ1550 line we measure a v_{black} (which corresponds to the wind terminal velocity v_∞; Prinja, Barlow & Howarth 1990) of $(900 \pm 150)\,\mathrm{km\,s^{-1}}$ (Fig. 2). We notice how this value is much larger than anything implied by the optical linewidths and P Cygni features (which is why Leuenhagen & Hamann 1998 adopted a much lower value for v_∞ of $400\,\mathrm{km\,s^{-1}}$). This is likely to be a consequence of a particularly low wind density.

5.1.1 *The Balmer lines*

DBS97 noted that the Balmer line shapes of the PNe around the two [WC] central stars CPD −56°8032 and He 2-113 have a broad pedestal. Leuenhagen, Hamann & Jeffery (1996) determined an upper limit for the *stellar* hydrogen abundance by fitting this pedestal with synthetic profiles from their non-local thermodynamic equilibrium (non-LTE) code. However, DBS97 pointed out that the same broad pedestal was present at the base of *forbidden* lines, which are entirely of nebular origin. This indicates that either a complex nebular velocity field is the cause of the irregular nebular line shapes and of the pedestals at the base of the Balmer

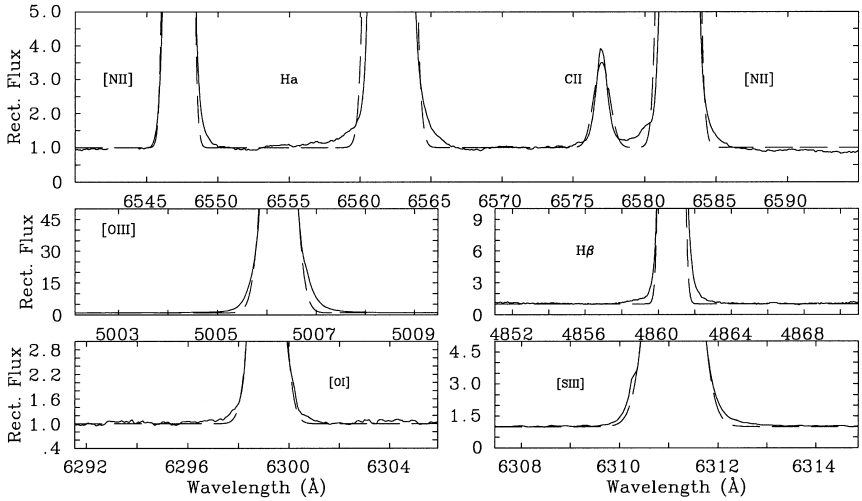

Figure 3. Gaussian fits to nebular lines, showing the nature of the asymmetry at their bases to be of nebular or instrumental origin.

lines, or perhaps more likely, the pedestals observed at the base of these strong lines is due to the grating instrumental profile.

Since the presence of hydrogen in cool [WC] central stars would give a clue about their origin, we have investigated the nebular lines of SwSt 1. In Fig. 3 we present Gaussian fits to Hα and Hβ, along with other forbidden lines. Although the Balmer lines do present a base which is broader than the Gaussian fit, many other nebular lines, i.e., [N II] $\lambda\lambda$6548,6583 and [O III] λ5007, have a similar shape. There is therefore no conclusive evidence for the presence of stellar hydrogen. In Section 5.5 we demonstrate how a hydrogen abundance of 10 per cent (by mass) as determined by Leuenhagen & Hamann (1998) is not inconsistent with our own fits.

5.2 Description of the model codes

The code adopted to carry out the stellar analysis is the improved Sobolev approximation code ISA-Wind (de Koter, Schmutz & Lamers 1993; de Koter, Heap & Hubeny 1997). This modelling program solves the radiation transfer equation under the condition of statistical equilibrium in a spherical, extended atmosphere. The line radiation transfer is implemented using an improved version of the Sobolev approximation, which has been shown to be appropriate for the thick atmospheres of Wolf–Rayet stars (de Koter et al. 1997; Crowther et al. 1999; De Marco et al. 2000).

The wind of SwSt 1, however, is less dense than the winds of most Wolf–Rayet stars, as can be inferred from the overall weakness of its spectral lines. This indicates that the inner, slow-moving parts of the stellar atmosphere are exposed in this region, and the Sobolev approximation might break down. To check on the results obtained with ISA-Wind, we used the comoving frame code CMFGEN (Hillier & Miller 1998). CMFGEN confirmed the results obtained with ISA-Wind. However, some of the differences between the two codes are instructive, and although in what follows we refer mostly to ISA-Wind, results obtained using CMFGEN are presented alongside.

Line blanketing is included in the ISA-Wind model by a Monte Carlo approximation, which includes millions of spectral lines. This is described in detail by Schmutz et al. (1991). Comparison tests have been carried out (Crowther et al. 1999; De Marco et al. 2000) and show the technique to compare reasonably well to a detailed line-blanketing calculation carried out with CMFGEN (Hillier & Miller 1998), although the flux shortwards of 400 Å was too hard in the Monte Carlo technique.

Table 6. Summary of the atomic model adopted in our ISA-Wind non-LTE simulations of SwSt 1's stellar wind.

Ion	# Levels	Upper Level	# SL	SL Grouping	Dielectronic
H I	15	–	–	–	–
He I	19	^{1}P $n=4$	32	$n=20$ sing/trip	–
He II	20	–	–	–	–
C II	36	^{2}G $n=3$	2	thr. doub/quart	26
C III	31	^{1}S $n=5$	8	thr. sing/trip	31
C IV	9	^{2}F $n=4$	3	$n=7$	–
N I	3	^{2}P^o $n=2$	–	–	–
N II	29	^{3}S $n=2$	–	–	–
N III	11	^{2}D $n=3$	3	$n=4$ doub/quart	–
N IV	12	^{1}D $n=3$	–	–	40
N V	14	^{2}D $n=6$	–	–	–
O I	2	^{3}S^o $n=3$	–	–	–
O II	3	^{2}P^o $n=2$	–	–	–
O III	41	^{5}S^o $n=3$	–	–	–
O IV	11	^{2}D $n=3$	3	$n=4$ doub/quart	–
O V	12	^{1}D $n=3$	–	–	34
Si II	7	^{2}P $n=4$	–	–	–
Si III	16	^{3}F^o $n=4$	2	$n=5$ sing/trip	–
Si IV	12	^{2}G $n=5$	1	$n=6$	–
S III	11	^{3}P^o $n=3$	–	–	–
S IV	7	^{2}S^e $n=4$	–	–	–
S V	7	^{1}S $n=3$	–	–	–
S VI	7	^{2}F^o $n=4$	–	–	–

5.2.1 *The model atom*

The number of atomic levels included in the calculation influences the line strengths. Ideally, one would want to employ as many lines as possible of as many elements as possible. Unfortunately, the larger the atomic model the slower the calculation. As a result, a compromise has to be adopted. The atomic model used by our ISA-Wind calculation uses Opacity Project data (Seaton 1995) and is summarized in Table 6. The use of superlevels (SLs) reduces computational times, while at the same time including high-lying levels. SLs are groups of levels within which populations are calculated in LTE. The grouping scheme changes for different ions. In Table 6 we indicate the scheme used: '$n=4$' means that all

levels up to and including principal quantum number 4 are included; 'sing/trip' means that singlets and triplets are grouped separately; 'thr.' indicates that enough SLs were constructed to include all levels listed in the Opacity Project data base up to the ionization threshold. The effect of slight variations in our grouping scheme (as well as the total number of SLs) on the synthetic lines was studied for the cases of C II and C III, and found not to alter the synthetic lines. Only helium, carbon, oxygen, silicon and iron are all included explicitly in the CMFGEN calculation, but in somewhat greater detail than in the case of ISA-Wind.

5.3 Photon loss

'Photon loss' is the name given by Schmutz (1997) to the interaction between the photon field of the He II Lyα line at 303.78 Å and nearby metal lines (e.g., the O III Bowen lines at 305.72 and 303.65 Å). This can be responsible for a decrease in the ionization equilibrium of the wind with respect to the equilibrium obtained when no such line–line interaction is accounted for. In order to fit the observed spectrum when photon loss is included in the model, the model's stellar temperature has to be higher, which results in a higher spectroscopic luminosity. This contributes to a lower wind performance number, and allowed Schmutz (1997) to calculate a velocity structure for the outer wind of WR6.

De Marco et al. (2000) implemented this approximation in the Sobolev code ISA-Wind, and showed that results were similar to those obtained using the code CMFGEN (for the WC8 stellar component to the γ Velorum binary), where line–line interaction is taken into consideration explicitly. Here we have used the 'photon-loss' option, which resulted in only a slightly higher effective temperature ($\sim$2000 K). The effect has been shown by Schmutz (1998) not to be important in the case of O stars, which have weaker winds. This also seems to be the case for the weaker wind of SwSt 1. CMFGEN naturally includes line–line interaction, and therefore 'photon-loss' is automatically taken into account (De Marco et al. 2000).

5.4 Stellar modelling technique

Traditionally, modelling of WR stars starts with matching a subset of the observed He I and He II lines with model line profiles, from which approximate values for the effective temperature and mass-loss rate of the star are determined. The metal abundances are then varied, to afford fits to a representative sample of their lines. Even in modern calculations the velocity law is seldom varied from either a simple or a composite beta-law (e.g. Hamann & Koesterke 2000).

A weakness of this technique is that in a significant number of cases, the choice of diagnostic lines determines what parameters are derived. If excellent fit quality can be obtained for a large number of lines, this gives confidence in the derived parameters, but if only a small subset of the observed lines can be fit by any given model, the parameters are only as good as the choice of diagnostics. Additionally, running non-LTE line-blanketed codes is very time-consuming, so that once a reasonable match to a set of lines is achieved, different parameter spaces are seldom explored to determine whether other parameter sets fit the emission lines to a similar degree of accuracy.

The fast calculation speed of the ISA-Wind code allowed De Marco et al. (2000) to show that similar synthetic spectra can sometimes be obtained with different combinations of temperature and mass-loss rate. When only a poor fit quality is achieved, or when only a subset of the diagnostic lines is fit simultaneously, it might be hard to choose which model best represents the star, leading to a degeneracy.

The spectrum of SwSt 1 presents a formidable challenge for spectral synthesis, in that it is impossible to fit all the diagnostic lines simultaneously. As a result, it is possible to derive different model parameters depending on which diagnostic lines we decide to include. The exploration of a vast parameter space (stellar temperature, mass-loss rate and metal abundance), made possible by our fast code, together with the use of observational constraints not usually coupled with non-LTE analyses, enabled us to gain a reasonable confidence in our final choice of stellar parameters. Our choice of diagnostic lines comprised all lines included within the levels of our model atom, leaving out those between high-lying levels which might be under-populated. For helium we used He II λ4686 (λ5411 is blended with nebular a [Fe II] line, and can only be used as an upper limit) and He I λ5876,4471,6678. As pointed out above, there is extremely little He I in this star, if any, so that the lines (severely blended with nebular components) could be used only to impose an upper limit on their strengths. To constrain the ionization equilibrium, one has to appeal to carbon: C II λ4267, C III λ5696 and λ8500, and C IV $\lambda\lambda$5801,12 and λ5470 were employed. These lines are also used to determine the carbon abundance. To constrain the oxygen abundance we used O III λ5592 (all other lines are too weak or dominated by the nebula).

Once the diagnostic lines were chosen, an approximate value for the temperature and mass-loss rate was obtained, for which reasonable fits were achieved. Since no combination of T_*, $\dot{M}$ and carbon abundance fitted the spectrum to a satisfactory level, in that the synthetic lines were always too broad in the core and too narrow at the base, we experimented with different velocity laws. In particular, we tested velocity laws with progressively slower flows in the inner regions, so as to reduce the linewidths, maintaining the observationally derived value of v_∞. The electron density change induced by the different laws changes the wind opacity, with a repercussion on the ionization equilibrium of the star, and therefore on the line intensities. Consequently, different basic parameters are implied by different velocity laws.

5.5 Stellar model results

Model fits to the stellar spectrum of SwSt 1 are presented in Fig. 4 (thick and thin solid lines for ISA-Wind and CMFGEN models, respectively, and dotted lines for the observations), while the model parameters are presented in Table 7, together with the results of Leuenhagen & Hamann (1998), scaled to our adopted distance. In what follows we discuss the results obtained with the modelling code ISA-Wind, followed by a discussion of additional results obtained with the code CMFGEN.

5.5.1 ISA-Wind

He II λ4686 is well reproduced, while He II λ5411 and He I $\lambda\lambda$5876,6678, and other lines which suffer blending with nebular emission, are within reasonable limits. Other synthetic He II lines (e.g., λ4542 and λ4200) are in absorption with wide wings. Since these wings are not observed, and He I lines are mostly of nebular origin, we have not used these lines as diagnostics.

C IV $\lambda\lambda$5801,12 are over-predicted, C IV λ5470 is well matched, while C IV λ4441 is somewhat weak. In order to fit C IV $\lambda\lambda$5801,12 the effective temperature could not be higher than 35 kK, no matter what other parameters are adopted. However, at this temperature

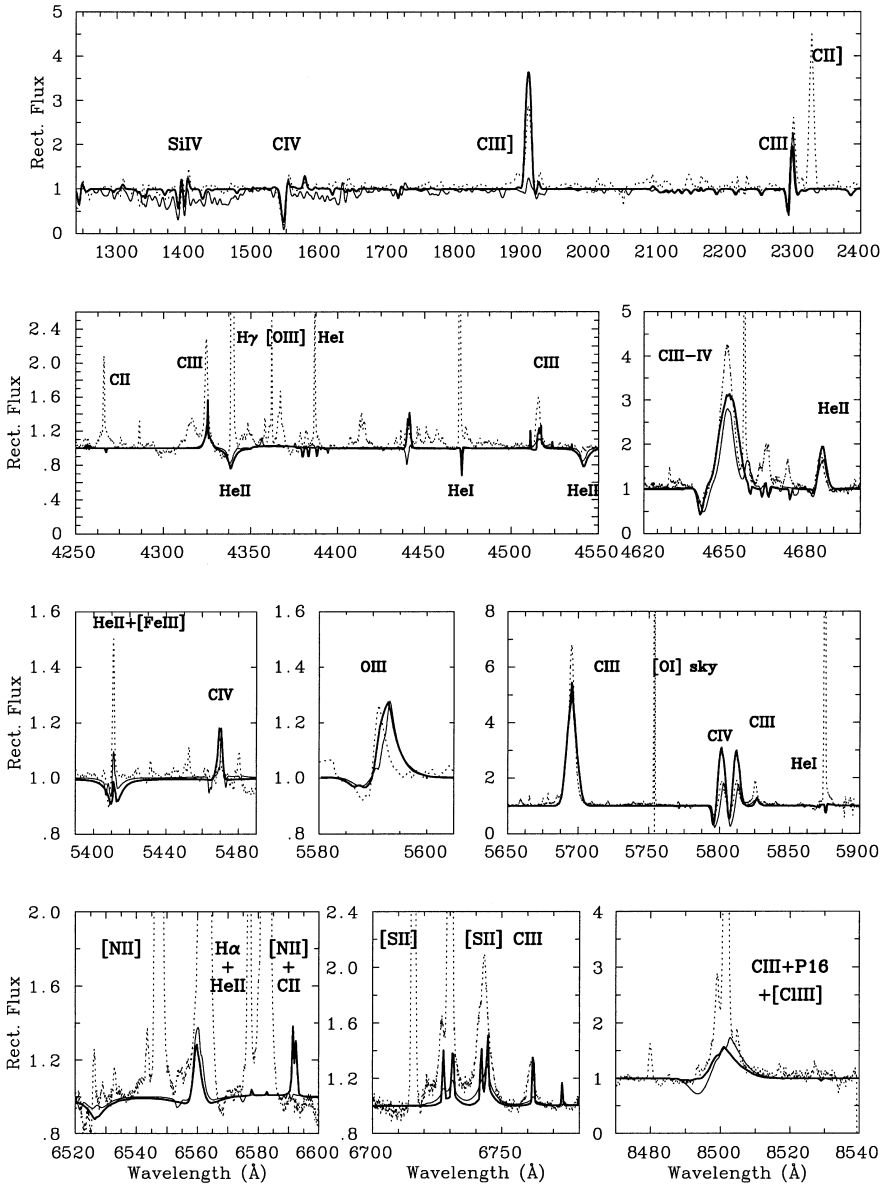

Figure 4. ISA-Wind model fits (thick solid line) to the optical and UV stellar rectified spectrum of SwSt 1 (dotted line). The CMFGEN models fits (thin solid line) are presented alongside.

Table 7. Stellar parameters from our non-LTE models (ISA-Wind and CMFGEN), compared with those of Leuenhagen & Hamann (1998; LH98), before and after scaling them to our own adopted distance.

V (mag)	$E(B-V)$ (mag)	D (kpc)	M_V (mag)	T_* (kK)	R_* ($R_\odot$)	log ($L/L_\odot$)	log ($\dot{M}/M_\odot\,yr^{-1}$)	v_∞ (km/s)	η	β_H %	β_{He} %	β_C %	β_O %	β_N %	Ref.
11.48	0.46	2.0	−1.45	40	2.0	3.95	−6.72	900	0.9	<10[a]	37	51	12	∼0	ISA−Wind
11.48	0.48	2.0	−1.51	46	1.5	3.95	−6.84	800	0.6	0	53	32	15	0	CMFGEN
11.9	0.41	1.4	−1.10	35	1.0	3.27	−6.90	400	1.3	<10	44	53	3	<0.5	LH98
–	–	2.0	−1.45	35	1.4	3.49	−6.79	400	1.3	<10	44	53	3	<0.5	LH98 scaled

[a] Limit from model profile fitting does not include possibility of blend with nebular emission (see text).

the λ5470 line is in weak absorption. C IV λ5470 has a better-understood formation mechanism compared to λλ5801,12 (Hillier & Miller 1999; Dessart et al. 2000) and was therefore given priority in the fitting procedure. Additionally, at 35 kK the fit to the C III λ4650 line is much worse, with the synthetic line too weak. C III λλ5696,8500 are also well matched by the model but C II λ4267 is poorly matched, with the model line being much too weak. However, the C II λλ6578,6583 blend has a very reasonable fit (C II λλ7231,7236 is severely affected by telluric absorption and blending with nebular emission line components and was therefore not fitted). The problem with C II λ4267 might be linked to insufficient levels in the atomic models. However, we have

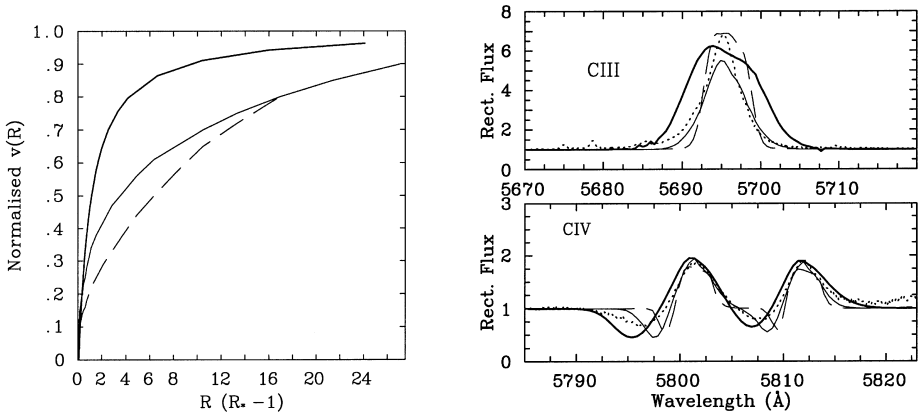

Figure 5. Left panel: alternative velocity laws compared to a $\beta = 1$ law (thick solid line). The adopted law (thin solid line) significantly improved the line fits, making lines broad at the base and narrow in the core, and reproduced the position of their P Cygni absorptions, while the other laws produced lines which were too broad or too narrow. **Right panel**: ISA-Wind profile fits to C III λ5696 (top) and C IV $\lambda\lambda$5801,12 (bottom). The dotted line represents the data, the thick solid line represents the model calculated using a $\beta = 1$ velocity law, the thin solid line represents the model with the velocity law used for the final model of this paper, and the dashed line shows the slowest velocity law attempted. Model parameters are adjusted to fit the peak intensity of C IV $\lambda\lambda$5801,12.

experimented with more levels and included a considerable number of SLs and dielectronic recombination lines. Since a much stronger synthetic λ4267 (obtained by lowering the effective temperature) would lead to over-fitting $\lambda\lambda$6578,83, we still suspect the model atom is the reason for the problem. If a cooler stellar temperature is used to try and enhance C II λ4267, all fits deteriorate, even if the mass-loss rate is reduced to restore the He I/He II equilibrium. Increasing the mass-loss rate so as to enhance recombination of C III to C II, and so increase the strength of the C II λ4267 line, also fails. A higher mass-loss rate is also excluded by the fact that by increasing its value by 0.1 dex from the value reported in Table 7, all model lines of C III acquire deep P Cygni absorptions, which are not observed. Additionally, the He I lines increase in strength, in a way that cannot be compensated for by a larger temperature without losing the C III/C IV balance.

Increasing the carbon abundance, in steps, from C/He $= 0.2$ to 3 (by number), while adjusting other parameters, does not achieve an improvement in the fits. On the other hand, once the effective temperature and mass-loss rate have been determined, the C/He ratio can be determined with a 50 per cent accuracy. Even with the highest carbon abundance, the C II line did not increase for the temperature regime which satisfied the other lines. Additionally, when enhancing the C/He ratio the ionization equilibrium of the star is upset in such a way that He II lines are drastically decreased, which results in having to increase the temperature, at which point other carbon lines do not fit any more, most noticeably C IV $\lambda\lambda$5801,12, whose excitation is almost entirely dependent on temperature.

Returning to the C III line blend at 4650 Å, and to line shapes in general, we have used a velocity law which is slower than $\beta = 1$ in the inner parts of the wind (in accordance with that found by Hillier & Miller 1998, Crowther et al. 1999 and De Marco et al. 2000). For every parameter set, we tested a number of velocity laws with progressively slower winds in the inner parts of the flow. These are shown in Fig. 5. The slower the velocity law, the stronger and narrower the lines become (for identical stellar parameters). As a result, each adopted velocity law implied a new set of parameters, resulting in a trend of a somewhat cooler stellar temperature and lower mass-loss rate for slower velocities. For the slower velocity laws, narrower line profiles were accompanied by more redward-displaced P Cygni absorptions. As a result, it was relatively easy to choose the best velocity law from the position of the P Cygni absorption (as well as the overall linewidth and shape) of lines such as C III λ4650 and C IV $\lambda\lambda$5801,12. The velocity law which matched the position of the P Cygni profiles is marked as a thin solid line in Fig. 5 (left-hand panel) and can be parametrized following the formula of Hillier & Miller (1998) with $v_{\rm ext} = 500\,{\rm km\,s^{-1}}$, $v_\infty = 900\,{\rm km\,s^{-1}}$, $\beta_1 = 1$ and $\beta_2 = 8$. This resulted in the best match to the line shapes. In Fig. 5 (right-hand panel) we present profile fits obtained using a $\beta = 1$ law, and two slower laws. The model parameters were adjusted in each case to reproduce the line's peak intensity. As can be seen, the $\beta = 1$ law generates profiles which are too broad, while the dot-dashed line produces profiles too narrow at the base but too broad in the core.

In summary, although the fits presented in Fig. 4 (thick solid line) are not excellent, there is no other parameter combination of mass-loss rate, temperature and C/He number ratio[4] which would satisfy the observed spectrum to a higher degree of accuracy. The derived quantities and their errors are therefore the following: $T_* = (40\,000 \pm 2000)$ K, $\log(\dot{M}/{\rm M_\odot}) = (-6.72 \pm 0.1)$, C/He $= (0.46 \pm 0.20)$ and O/He $= (0.08 \pm 0.02)$ (by number). The wind performance number η [$= L/(\dot{M}v_\infty c)$] is 0.9, indicating that the wind of SwSt 1 can be driven radiatively in the single scattering limit. The derived stellar luminosity of 8900 $L_\odot$ is towards the high end for a PN central star (implying a relatively large stellar mass). It is difficult to determine the mass which corresponds to this luminosity, since the highest core mass for which Vassiliadis & Wood (1994) calculated Milky Way initial abundance helium-burning tracks was 0.63 $M_\odot$, but inspection of their fig. 8 indicates that our derived luminosity for SwSt 1 at 40 000 K is only slightly above the LMC-abundance evolutionary track for a 0.679-$M_\odot$ core mass.

The helium, carbon and oxygen abundances are 37, 51 and 12 per cent by mass, respectively, implying a C/O mass ratio of 4.3. The oxygen abundance in particular is obtained from fitting the O III line at 5592 Å. The lower and upper limits for the O/He ratio allowed by the fit of the λ5592 line are 9 and 15 per cent. Additional uncertainty derives from fitting a single line. We note that if a lower effective temperature were to be adopted, the oxygen

[4] The parameter space explored spanned from 30 to 45 kK in stellar temperature, $\log(\dot{M}/{\rm M_\odot}) = -6.0$ to -6.7, and C/He $= 0.2$ to 3.0.

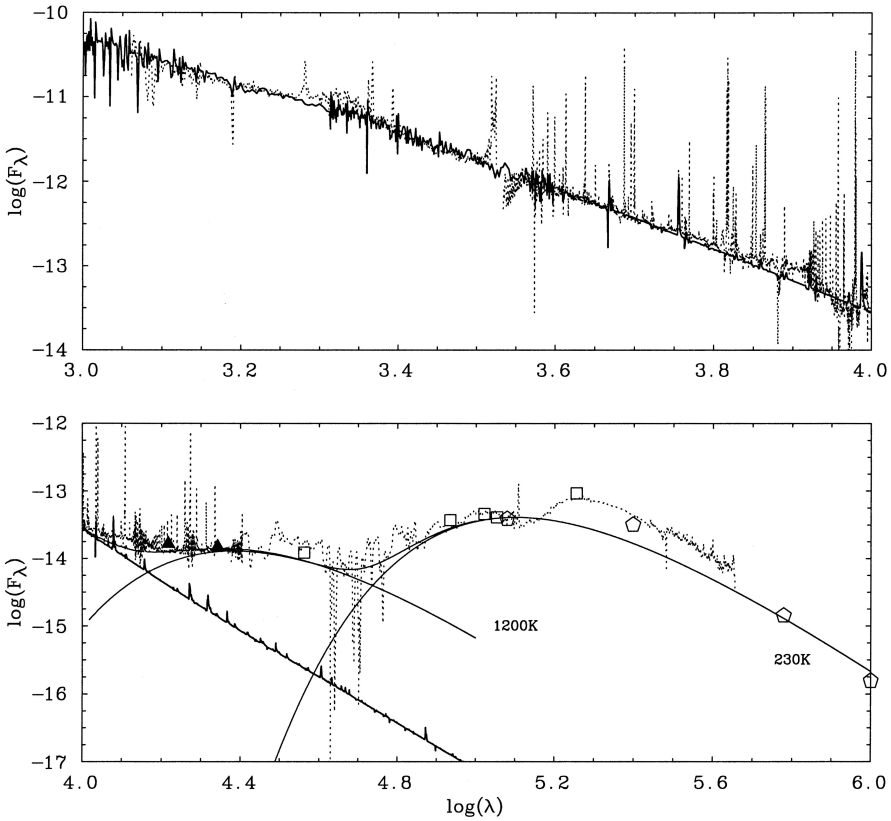

Figure 6. Top panel: the dereddened ultraviolet (*IUE*), optical (UCLES) and near-infrared (SOFI) spectra of SwSt 1 (dotted line), compared with the best-fitting ISA-Wind stellar model (solid line). **Bottom panel**: the near-infrared (SOFI) and mid-infrared (*ISO* SWS) energy distribution of SwSt 1 (dotted line) compared to the flux distribution from the best-fitting ISA-Wind stellar model (solid line, $\log\lambda < 4.4$) and 1200- and 230-K blackbody curves (solid line, $\log\lambda > 4.4$). Ground-based infrared photometry (Allen & Glass 1974; Cohen & Barlow 1974) and colour-corrected *IRAS* fluxes are also plotted (square symbols). Wavelength units are Å, and flux units are erg cm^{-2} s^{-1} Å^{-1}.

abundance determined by a fit to this O III line would be higher still.

In Fig. 6 we show the ISA-Wind synthetic spectrum, compared with the IR, optical and *IUE* dereddened data. A slight over-compensation of the 2200-Å feature by the adopted $E(B-V) = 0.46$ is not considered worrying in view of the known variations in the relative strength of this feature (Mathis 1994), since the overall continuum slope is well matched by our *V*-scaled synthetic spectrum (if we make an exception for the far blue and red edges of the optical spectrum). By adopting reddening values as low as 0.30 (which nulls the 2200-Å feature) the continuum slope is clearly too gentle to match the model, while for a reddening value of 0.50 the slope will be too steep. In Fig. 6 we also plot the near-IR SOFI spectrum (scaled to the *J* magnitude of Allen & Glass 1974 and colour-corrected *IRAS* photometry values, together with blackbody curves with temperatures 1200 and 230 K. These curves indicate that some of the dust around this PN is very hot. This is in agreement with the study of Zhang & Kwok (1991).

5.5.2 *CMFGEN*

The fit quality obtained with the code CMFGEN is very similar to that obtained with ISA-Wind. Although some lines are better reproduced (e.g., C IV λλ5801,12) others are somewhat worse (e.g., C IV λ4441). The broad He II absorption lines wings obtained with ISA-Wind are somewhat narrower in the models fits of CMFGEN, in better agreement with the data. C III λ1909 is weaker and more in agreement with the observations (note that in Fig. 4 this line is a

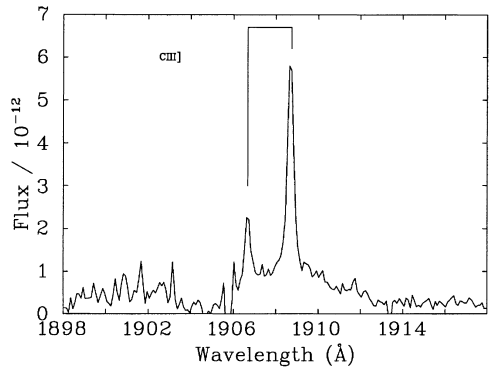

Figure 7. The high-resolution *IUE* spectrum of SwSt 1 showing the semiforbidden stellar-nebular blend of C III] λλ1906,1909.

blend of stellar and nebular components, as can be appreciated by inspecting Fig. 7). On the other hand, the shape of the C III–IV blend at ∼4650 Å is somewhat worse in the CMFGEN fits, and the C III line at 8500 Å has an unobserved P Cygni absorption. The fit to the only oxygen diagnostic line, i.e., O III λ5592, is similar to the one obtained with ISA-Wind. The stellar parameters obtained with CMFGEN are presented alongside those obtained with ISA-Wind in Table 7. Overall, the derived stellar parameters for SwSt1 using CMFGEN match closely with those from ISA-wind, except that the stellar radius is smaller, implying a higher stellar temperature of 46 kK. The mass-loss listed in Table 7 does not consider clumping.

Almost identical fits can be obtained with a filling factor of 10 per cent with clumping starting at $v = 100\,\mathrm{km\,s^{-1}}$. In this case the mass loss is $7 \times 10^{-8}\,\mathrm{M_\odot\,yr^{-1}}$, or a factor of 2 lower than obtained without clumping. Due to the relatively low wind density, the electron scattering wings cannot be used to constrain the clumping. The only noticeable changes are in C III λ9710 and λ1909 where clumped models give 20 per cent weaker emission. However, since the latter is dominated by the nebula and the former is included only in our low-resolution SOFI data, these cannot provide any useful constraint.

The only considerable difference between the modelling efforts with ISA-Wind and CMFGEN is that the stellar abundances are discrepant (Table 7). This is possibly due to the different cocktail of atomic data used by the model codes, although, as is frequent with complex non-LTE codes, it might also be due to a mix of factors hard to trace. In particular, the carbon and oxygen mass fractions are 32 and 15 per cent, respectively, compared to ISA-Wind's 51 and 12 per cent. This translates into a C/O mass ratio of 2.1 for CMFGEN versus 4.3 for ISA-Wind. Both CMFGEN and ISA-Wind values are higher than solar (∼0.4). The maximum value that the C/O ratio can attain according to the models (Herwig 1999), is the intershell value, ∼4. So, although both values are acceptable, the ISA-Wind value would imply an extremely effective third dredge-up.

We obtain a good fit of the CMFGEN model flux distribution to the dereddened data, although a slightly higher value of the reddening [$E(B-V) = 0.48$ mag] had to be adopted.

5.5.3 Comparison with the analysis of Leuenhagen & Hamann 1998

Leuenhagen & Hamann (1998) present fits to their 1-Å-resolution optical spectrum that are not dissimilar in quality from our own, although they fit a smaller spectral range. The effective temperature of 40 kK derived with the ISA-Wind modelling code, is higher than their 35 kK. Our mass-loss rate is similar to the one derived by Leuenhagen & Hamann (once the different distances are taken into account), while our final wind velocity is more than twice as large. Leuenhagen & Hamann have not determined v_∞ from the C IV line, limiting themselves to fitting the widths of the optical lines. We have already seen how these lines are peculiarly narrow and in apparent disagreement with the value indicated by the P Cygni absorption of C IV λ1550. Inspecting their fig. 3, we notice that their model optical lines are too narrow and suffer from the same problem as our fits with a $\beta = 1$ velocity law.

The hydrogen abundance of 10 per cent (by mass) determined by Leuenhagen & Hamann (1998) as an upper limit, when used in our model, produces a synthetic Hα-He II line blend which is not entirely in disagreement with our observations. Therefore, based *solely* on this fit, we confirm their determination. On the other hand, as already noted in Section 5.1.1, the shape of the blend might be due to either nebular emission or the instrumental profile, since nebular forbidden lines exhibit the same pedestal. Our ISA-Wind carbon abundance is similar to that determined by Leuenhagen & Hamann (1998), while the carbon abundance obtained with CMFGEN is lower. Our oxygen abundance, obtained with either of the two codes, is higher than the abundance derived by Leuenhagen & Hamann.

6 NEBULAR ABUNDANCE ANALYSIS

6.1 Nebular line fluxes

The nebular spectrum of SwSt 1 is much stronger and slightly higher in excitation than those of the PNe with [WC10] central stars analysed by DBS97 and De Marco & Crowther (1998). Many nebular He I lines could be measured: amongst them we selected those at 4471.5, 5875.7 and 6678.1 Å, disregarding the line at 7065.2 Å due to its being dominated by collisions and the possibility that it is affected by telluric absorption. The [O II] line complex at 7325 Å is made up of four lines with wavelengths of 7318.8, 7319.9, 7329.6 and 7330.6 Å, where the individual components are partly blended. Unfortunately, the blend at 7319 Å was affected by an echelle order join which removed a part of the flux. In order to obtain a measurement of the flux in those lines, we therefore snipped the section containing the join. The snipped line, despite missing the central part, still had clearly identifiable wings and could therefore be successfully fitted with a Gaussian. We none the less decided to assign a 50 per cent uncertainty to it, and did not use it in any of the parameter determinations. The [O II] lines at 3726.0 and 3728.8 Å are resolved and completely unblended with any stellar feature. [O III] lines appear at 4363.2, 4958.9 and 5006.8 Å.

All four [S II] nebular lines included in our wavelength range could be measured, namely the lines at 4068.6, 4076.3, 6716.5 and 6730.8 Å. The line at 4068.6 Å was found to lie on an order join. However, since abundance results obtained with it or with the weaker lines at 4076.3 Å were very similar, we decided to treat it normally and only assign it a marginally higher uncertainty. To determine the abundance of S^{2+}, we used λ9531.0. The telluric water vapour line at 9069.126 Å affects the measurement of the [S III] line at 9068.9 Å, since its measured ratio to the λ9531 line is 0.28, lower than the theoretical ratio of 0.403.

Three lines of singly ionized nitrogen reside in our spectral range, but as the [N II] ratio λ6583/λ6548 was equal to 1.4, instead of 2.90, we decided that the strong λ6583 line was saturated (as was Hα) and did not include it in any of our determinations. Together with the λ6548 line, we used [N II] λ5755.

To derive the nebular C/H ratio, we used *IUE* observations of the semiforbidden C II] λ2326 and C III] λ1909 lines. We assume the stellar contribution to λ2326 to be negligible, while we could deblend the stellar and nebular contributions to C III λλ1906,1909 using the high-resolution *IUE* spectrum (Fig. 7).

Besides the lines listed in Table 8, we identify forbidden lines of Fe^+ (e.g., [Fe II] λ4606), Fe^{2+} (e.g., [Fe III] λ4881) and possibly Fe^{3+} (e.g., [Fe IV] λ5677). We also identify [Ne III] λ3868, [Ar III] λ5191.8 λ7135.8 (affected by an order join) and λ7751.1 and [Cl III] λ5517.7 and λ5537.9. A line list is presented in Appendix B.

6.2 Nebular temperature, density and abundances

In Fig. 8 we plot a nebular diagnostic diagram for SwSt 1. From a weighted mean of the diagnostic lines we adopt values for the electron temperature and density of 10 500 K and 31 600 $\mathrm{cm^{-3}}$ ($\log N_\mathrm{e} = 4.5$), respectively (Table 9).

The temperature implied by the [O III], [S III] and [Ar III] diagnostic ratios is between 11 000 and 10 000 K for electron densities between 10^3 and $10^5\,\mathrm{cm^{-3}}$. The C III] λ1909/λ1906 ratio of 0.34 indicates $\log N_\mathrm{e} = 5.1$ for T_e in the range 9000–14000 K. However, this line ratio is severely affected by the blend with the stellar component. Deblending by fitting nebular and stellar components to the doublet resulted in a large uncertainty.

The diagnostic ratios from singly ionized elements seem to agree on a lower density ($4.0 < \log N_\mathrm{e} < 4.5$), if we make an exception for the [O II] ratio λ3727/λ7330. This ratio uses lines from two different grating settings and therefore might be affected by errors

Table 8. Observed (F_λ) and dereddened [I_λ; $E(B-V)=0.46$] nebular line intensities for SwSt 1 from the 1993 UCLES spectrum. The dereddened Hβ flux is 1.50×10^{-10} erg cm^{-2} s^{-1}. Errors are gauged at 10 per cent. The rest wavelengths of the lines are from Kaufman & Sugar (1986). The spectral resolution is indicated at the beginning of each section.

Ion	λ_0 (Å)	FWHM (km s^{-1})	F_λ (ergs cm^{-2} s^{-1})	$100\times I_\lambda$ /I(Hβ)
		$\Delta v\sim900$ km s^{-1}		
C II]	2326	–	3.9×10^{-12}	97
		$\Delta v\sim30$ km s^{-1}		
C III]	1906.7	–	5.7×10^{-13}	13
C III]	1908.7	–	2.0×10^{-12}	38
		$\Delta v\sim20$ km s^{-1}		
[O II]	3726.0	44	6.51×10^{-12}	30.0
[O II]	3728.8	46	2.55×10^{-12}	11.7
[Ne III]	3868.8	40	3.35×10^{-14}	0.48
[S II]	4068.6	41	5.23×10^{-13}	2.2
[S II]	4076.3	41	2.05×10^{-13}	0.85
		$\Delta v\sim8$ km s^{-1}		
Hδ	4101.7	44	6.20×10^{-12}	24.7
Hγ	4340.5	41	1.19×10^{-11}	44.9
[O III]	4363.2	31	7.11×10^{-14}	0.27
He I	4471.5	38	6.96×10^{-13}	2.5
Hβ	4861.3	41	3.22×10^{-11}	100
[O III]	4958.9	34	3.80×10^{-12}	11.4
[O III]	5006.8	33	1.01×10^{-11}	29.5
[Ar III]	5191.8	33	1.38×10^{-14}	0.04
[N I]	5197.9	77	4.80×10^{-14}	0.13
[N I]	5200.2	73	2.91×10^{-14}	0.08
		$\Delta v\sim20$ km s^{-1}		
[O I]	5577.3	30	7.83×10^{-14}	0.19
[N II]	5754.6	28	1.42×10^{-12}	3.3
He I	5875.7	42	3.17×10^{-12}	7.1
[O I]	6300.3	49	7.43×10^{-13}	1.5
[S III]	6312.1	39	1.30×10^{-12}	2.6
[O I]	6363	49	2.45×10^{-13}	0.49
[N II]	6548.0	46	1.64×10^{-11}	31.1
He I	6678.1	39	9.26×10^{-13}	1.7
[S II]	6716.5	62	3.91×10^{-13}	0.72
[S II]	6730.8	55	7.92×10^{-13}	1.4
He I	7065.2	39	2.11×10^{-12}	3.6
[O II]	7318.6	–	3.96×10^{-12}:	6.4
[O II]	7319.4	–	4.35×10^{-11}:	70.7
[O II]	7329.6	33	8.36×10^{-12}	13.6
[O II]	7330.7	35	8.62×10^{-12}	14.0
[Ar III]	7751.1	34	7.13×10^{-13}	1.1
[S III]	9531.0	38	7.53×10^{-11}	90.7

in the flux calibration. However, if this were the cause of the discrepancy, we would also have to be wary of the [S III] λ9531/λ6312 ratio (which we have used above) and the [S II] λ4072/λ6725 ratios, although these employ the green and red settings and not the blue and red settings used by the [O II] λ3727/λ7330 ratio. The ratios [O II] λ3727/3729 and [S II] λ6717/6731 are unreliable because they are at their high-density limit. Therefore only [S II] λ4072/λ6725 yields a reliable density diagnostic. From [S III] λ6312/λ9531, [O III] λ4959/λ4363, [Ar III] λ7751/λ5192, [N II] λ5755/λ6548 and [S II] λ4072/λ6725 we derive $T_e = 10\,500$ K and $\log(N_e/\mathrm{cm}^{-1}) = 4.5$.

Although the *HST* images point to a somewhat stratified PN (with the [O III] image being smaller than the Hβ one), we feel inclined to average the results obtained from the singly and doubly ionized elements. SwSt 1 is a young and compact PN, and we therefore feel unjustified in using different electron density and temperature combinations for the singly and doubly ionized regions, a choice that is more appropriate for more extended, higher ionization objects.

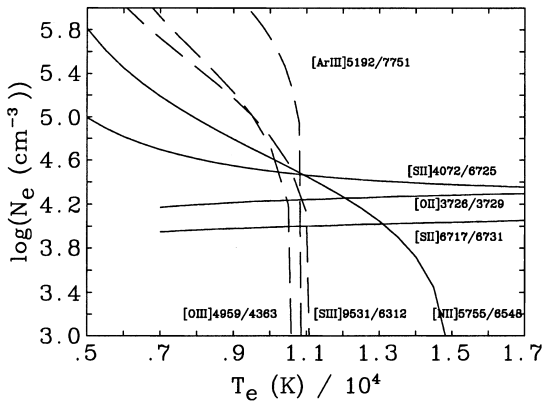

Figure 8. Diagnostic diagram, $\log(N_e)$ versus T_e, for SwSt 1. The solid lines are obtained from ratios of ions in the first stage of ionization, and the dashed lines are for ions in the second ionization stage.

Table 9. The nebular electron temperature and density adopted for SwSt 1, along with values from the literature.

T_e (K)	$\log(N_e)$	$E(B-V)$	Ref.
$10\,500\pm500$	4.5 ± 0.2	0.46	this work
$11\,400\pm500$	5.0 ± 0.1	0.41	dFPV87
8000	5.0 ± 0.1	0.34	FGC84

Table 10. Nebular ionic abundances for SwSt 1.

Ratio	Abundance	Lines Used
He^+/H^+	0.044 ± 0.004	He I $\lambda\lambda$4471,5876,
C^+/H^+	$1.21(-4)^a\pm0.60(-4)$	C II]λ2326
C^{2+}/H^+	$1.19(-4)\pm0.24(-4)$	C III]λ1909
N^+/H^+	$1.99(-5)\pm0.20(-5)$	[S II]$\lambda\lambda$5755,6548
O^+/H^+	$2.44(-4)\pm0.24(-4)$	[O II]$\lambda\lambda$3726,3729,7330
O^{2+}/H^+	$1.05(-5)\pm0.10(-5)$	[O III]λ4959
Ne^+/H^+	$9.77(-5)\pm1.19(-5)$	[Ne II] 12.8 μm^b
Ne^{2+}/H^+	$3.94(-6)\pm0.80(-6)$	[Ne III] λ3868
S^+/H^+	$2.96(-7)\pm0.30(-7)$	[S II]$\lambda\lambda$6713,6731,
S^{2+}/H^+	$4.23(-6)\pm0.80(-6)$	[S III]λ9531

$^a1.21(-4) = 1.21\times10^{-4}$.
^{b}line flux from Aitken & Roche 1982.

Flower et al. (1984) also derived $\log(N_e) = 5.0$ for SwSt 1 from the high-resolution *IUE* spectrum of the C III] $\lambda\lambda$1907,1909 diagnostic lines. They also quoted an upper limit for the electron density of 2×10^4 cm^{-3}, derived from the [O II] λ3729/λ3726 ratio (which is almost identical to ours); however, they argued that this ratio is too close to the high-density limit to be reliable. Their temperature determination, using the [O III] λ5007/λ4363 ratio, was 8800 K [for $E(B-V) = 0.70$], not inconsistent with our own value (although we employ a lower reddening, the effect is not major over such a short baseline). However, their determination using the [O III] λ5007/λ1663 ratio implies a higher electron temperature (15 000 K). If we ascribe the discrepancy to the use of two different spectra in the second determination (*IUE* and optical), which might have imperfect absolute flux calibrations, we can reconcile our own determinations of the temperature and density for the doubly ionized element with theirs. de Freitas Pacheco & Veliz (1987) derived $\log(N_e/\mathrm{cm}^{-3}) = 5.0$ and $T_e = (11\,400\pm500)$ K, from [S II] $\lambda\lambda$4068, 76/$\lambda\lambda$6716, 31, [O III]

Table 11. Empirical and modelled nebular abundances for SwSt 1 compared with mean values for Type-I and non Type-I PN from Kingsburgh & Barlow (1994).

Ratio	Abundance Empirical	Abundance Model[b]	Abundance Type-I	Abundance non Type-I
He^+/H^+	0.044 ± 0.004	0.04	0.129 ± 0.037	0.112 ± 0.015
log(C/H)+12	8.38 ± 0.25	8.40	8.48 ± 0.30	8.81 ± 0.30
log(*N*/*H*)+12	$7.32^a \pm 0.10$	7.99	8.72 ± 0.15	8.14 ± 0.20
log(O/H)+12	8.41 ± 0.20	8.15	8.65 ± 0.15	8.69 ± 0.15
log(Ne/H)+12	8.01 ± 0.07	7.88	8.09 ± 0.15	8.10 ± 0.15
log(S/H)+12	6.65 ± 0.10	6.62	6.91 ± 0.30	6.91 ± 0.30
C/O	0.94	1.79	0.68	1.32
N/O	0.08	0.08	1.17	0.28

[a] $\mathrm{ICF(N)} = \mathrm{O/O^+} = 1.05$, $\mathrm{N/H} = \mathrm{IFC(N)} \times \mathrm{N^+/H^+}$, following Kingsburgh & Barlow 1994.
[b] Abundances derived from the photoionization model, using the ISA-Wind WR stellar atmosphere as input (Table 12).

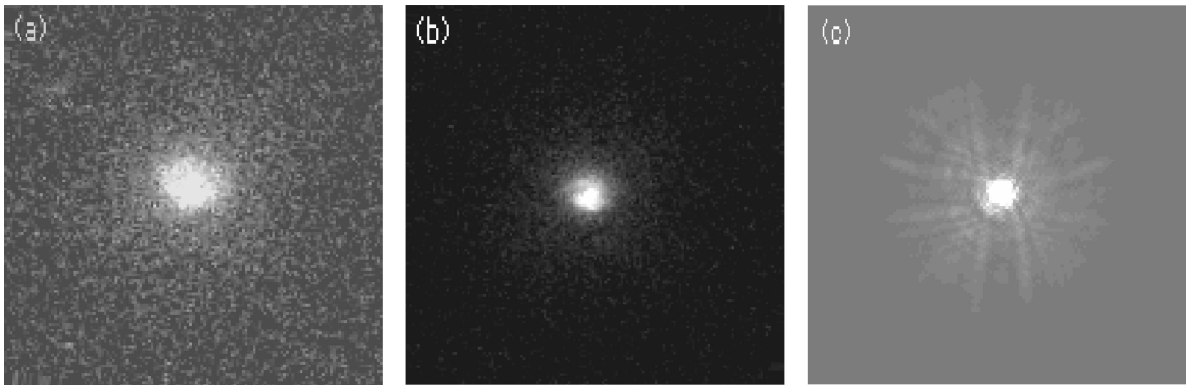

Figure 9. *HST* images of SwSt 1: (a) The average of the two raw Hβ images; (b) the average of the two raw [O III] images; (c) the synthetic point spread function generated by the program Tiny Tim. The FOV is 6 arcsec north is towards the top, and east to the left.

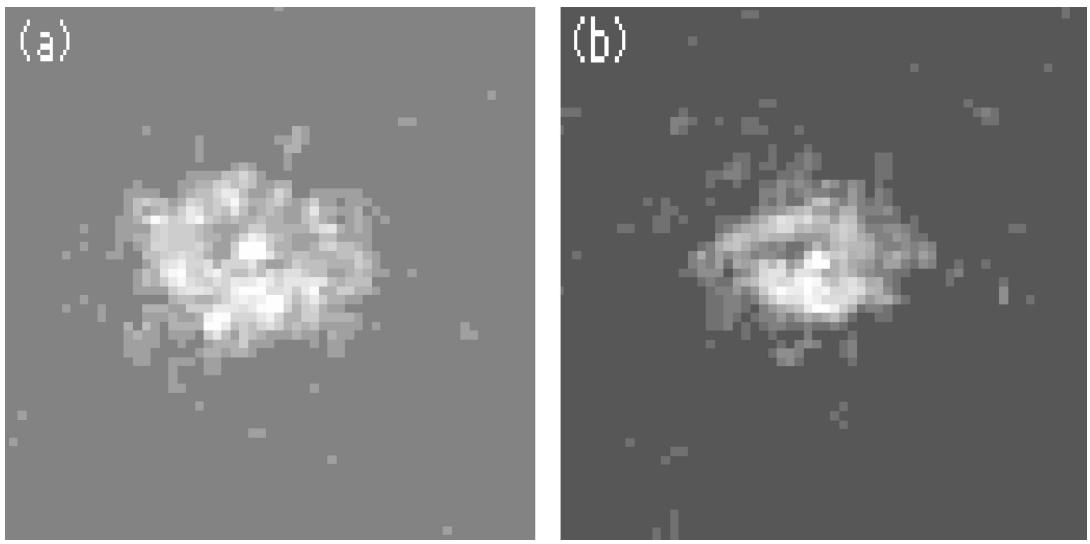

Figure 10. Deconvolved Hβ (a) and [O III] (b) *HST* images of SwSt 1; The images are displayed on a log scale; the field of view is 2.6 arcsec; north is towards the top, and east to the left.

$\lambda 4363/(\lambda 4959+\lambda 5007)$ and [N II] $\lambda 5755/\lambda\lambda 6548, 84$. Their diagnostic diagram is not inconsistent with our own.

Our derived abundances are listed in Tables 10 and 11, where they are compared with the mean values for Type-I and non Type-I PN from Kingsburgh & Barlow (1994). The quoted errors derive from errors on the flux measurements and do not take into account errors on the electron temperature and density. The C/H number ratio of 2.4×10^{-4} is not as high as for CPD $-$ 56°8032 (63×10^{-4}; DBS97), He 2-113 (50×10^{-4}; DBS97) or M 4-18 (12×10^{-4}; De Marco & Crowther 1999), and lower even than the mean PN value as determined by Kingsburgh & Barlow (1994; 5.49×10^{-4}). Additionally, with C/O = 0.94, SwSt 1 qualifies as

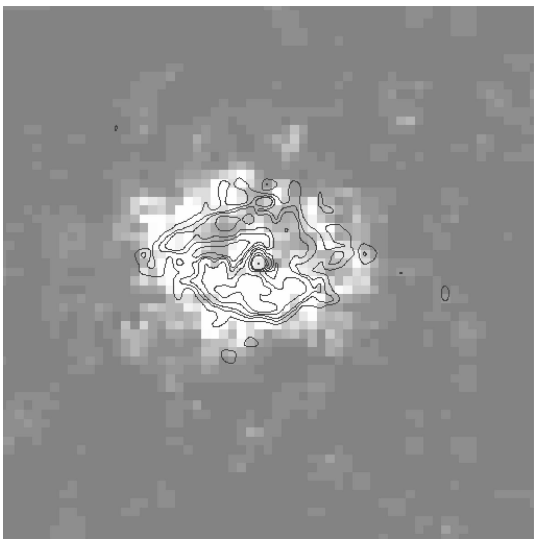

Figure 11. Deconvolved Hβ *HST* image of SwSt 1. Overplotted are the contours from the [O III] image (Fig. 10).

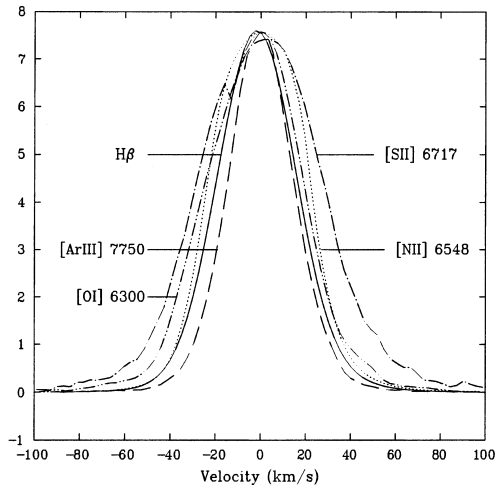

Figure 12. Comparison of selected nebular lines in the AAT–UCLES spectrum of SwSt 1. The lines are background subtracted and normalized to the peak intensity of the [Ar III] λ7750 line.

an O-rich PN. Flower et al. (1984) obtained C/O = 0.72, while de Freitas Pacheco & Veliz (1987) derived C/O = 0.54. The C/O ratio is consistent with the presence of a silicate emission feature at 10 μm (see Aitken & Roche 1982 and the SWS spectrum plotted in Fig. 6).

To obtain the N/H number ratio, we multiplied the N^+/H^+ ratio by an ionization correction factor of 1.05, obtained from the ratio of total oxygen to singly ionized oxygen abundances, in accordance with Kingsburgh & Barlow (1994).

7 *HST* IMAGES

Perek & Kohoutek (1967) quote an optical angular diameter of 5 arcsec, while Aaquist & Kwok (1990) measured a 5-GHz radio diameter of only 1.3 arcsec. No resolved optical image of SwSt 1 was found in the literature. SwSt 1 was observed in 1992 by *HST* in the Hβ and [O III] λ5007 lines, as part of a WF/PC snap-shot survey (two exposures per filter). These four pre-COSTAR images were already calibrated by the pipeline process (details can be found in the *HST* data handbook). DBS97 used the stellar [O III] images as a point spread function to deconvolve their images of CPD − 56°8032 and He 2–113. However, the nebula around SwSt 1 is more highly ionized than the ones around CPD − 56°8032 and He 2–113, as revealed by the prominent [O III] lines observed in our spectrum. Hence the [O III] image could not be used as a point spread function to deconvolve the Hβ image. We therefore used the program Tiny Tim (V4.0)[5] to create theoretical PSFs for the Hβ and [O III] images (the theoretical Hβ PSF is shown in Fig. 9 together with the raw images).

The deconvolved images of SwSt 1 (Fig. 10) reveal a broken ring of diameter $[(1.3 \times 0.9) \pm 0.2]$ arcsec, elongated in the east–west direction, in agreement with the radio images of Kwok, Purton & Keenan (1981) and Aaquist & Kwok (1990), but smaller than the 5 arcsec quoted by Perek & Kohoutek (1967). Although the images are of poor quality, this structure could be a ring whose plane is at about 30° from the line of sight. If we take 1.3 arcsec as the true diameter, a distance of 2.0 kpc and the expansion velocity of 21 km s^{-1} would imply a dynamical time-scale of 290 yr for the outer edge of the ionized material (although we do not know how far the neutral shell extends).

The [O III] image appears smaller than the Hβ image (about 75 per cent of the area), as can be seen from overlaying the normalized contours of the [O III] image on to the grey-scale plot of the Hβ image (Fig. 11). This is consistent with ionization stratification of the PN. Further confirmation of the stratified structure of this PN comes from analysing the nebular linewidths as a function of ionic charge (Fig. 12). After deconvolving the FWHM of individual lines with the respective instrumental profiles, nebular forbidden lines arising from singly ionized ions (e.g., [N II] λ6548 and [S II] λ6717), as well as lines coming from neutral ions (e.g., [O I] λ6300), are systematically broader (FWHM $\sim$ 45–60 km s^{-1}), while lines arising from doubly ionized ions (e.g., [O III] λ5007 and [Ar III] λ7750) have widths similar to the Balmer lines [FWHM(Hβ) = 40.2 km s^{-1}] or narrower (FWHM $\sim$ 30–40 km s^{-1}; see Fig. 12). This is consistent with the lines arising from higher ionization stages being formed in an inner, slower part of the PN, and the lines from lower ionization stages being formed further out in an accelerating part of the flow. The Balmer emission, coming from the entire ionized region, might have been expected to produce broader lines, although it might be more intense in the inner, denser region of the PN, yielding narrower profiles.

8 NEBULAR MODELLING

8.1 Zanstra temperatures

Following the formula of Milne & Aller (1975), for a 5-GHz flux of 243 mJy (the weighted average of Kwok et al. 1981, Milne & Aller 1982 and Aaquist & Kwok 1990; see Section 3.3), we predict an intrinsic Hβ flux of 8.07×10^{-11} erg cm^{-2} s^{-1}. This Hβ flux agrees within the uncertainties with the fluxes of Flower et al. (1984) for their adopted reddening of c(Hβ) = 0.68. From these dereddened Hβ fluxes and the distance of 2.0 kpc for SwSt 1 we derive a flux of hydrogen-ionizing photons for the star corresponding to $\log[Q_o(s^{-1})] = 46.90$.

We carried out a Zanstra analysis using blackbody as well as

[5] Tiny Tim is supported by the Space Telescope Science Institute; http://www.stsci.edu/software/tinytim/.

Table 12. Comparison of results from photoionization models for SwSt 1 with observations [$I(H\beta) = 100$], using ISA-Wind non-LTE, blackbody and Kurucz plane-parallel energy distributions.

Parameter	Observed	WR	Blackbody	Kurucz
$T_{\rm eff}$(K)	–	40.0	30.3	34.0
$\log(L/L_\odot)$	–	3.94	3.74	3.80
$R(R_\odot)$	–	2.0	2.7	2.3
$\log Q_0(s^{-1})$	46.90	47.53	46.90	46.90
$\log[I(H\beta)]$	−10.1	−10.1	−10.1	−10.1
$N_e(cm^{-3})$	31620	15000	31620	31620
ϵ	–	0.76	0.15	0.18
$R_{\rm inner}$(pc)	0.0086	0.0086	0.0086	0.0086
$R_{\rm outer}$(pc)	0.0252	0.0252	0.0252	0.0252
$M_{\rm PN}(M_\odot)$	–	0.021	0.009	0.015
τ(H I)	–	0.69	1.3	2.2
He/H	0.04	0.04	0.064	0.15
C/H×10^4	2.51	2.51	4.68	2.51
N/H×10^5	1.99	9.86	4.11	2.13
O/H×10^4	2.57	1.40	1.90	0.78
S/H×10^6	4.17	4.00	6.00	4.60
Ne/H×10^5	9.80	7.60	8.80	7.90
1909 C III]	71	68	33	14
2326 C II]	85	19	76	208
3726 [O II]	30	57	39	38
3729 [O II]	18	23	14	14
3868 [Ne III]	0.5	0.0	4.8	0.06
4068 [S II]	2.2	2.5	2.5	3.7
4076 [S II]	0.85	0.27	0.82	1.2
4363 [O III]	0.3	0.09	0.4	0.02
4471 He I	2.5	2.3	3.3	1.2
5007 [O III]	29	204	62	2.2
5755 [N II]	3.2	2.2	1.9	3.1
5876 He I	7.1	6.7	9.2	3.6
6300 [O I]	1.5	0.0	0.06	0.07
6363 [O I]	0.5	0.0	0.02	0.02
6548 [N II]	31	30	27	32
6678 He I	1.7	1.8	2.5	1.0
6717 [S II]	0.7	0.2	0.8	1.1
6731 [S II]	1.4	0.4	1.9	2.5
7325 [O II]	28	18	20	23
9532 [S III]	91	84	92	94
128 000 [Ne II]	68	67	65	67
C^{2+}/C^+	0.98	9.8	0.23	0.17
O^{2+}/O^+	0.043	0.81	0.18	0.088
S^{2+}/S^+	14	9.7	10.7	15
Ne^{2+}/Ne^+	0.040	–	0.063	0.004
$T_e(N^+)$(K)	10 500	10 500	9300	10 800

Kurucz ATLAS9 (Kurucz 1991) model atmospheres with $\log(g) = 4.0$, the minimum gravity tabulated for atmospheres of the required effective temperatures. We derive a blackbody H I Zanstra temperature of $(30\,300 \pm 500)$ K, while the ATLAS9 model grid yields an effective temperature of $(34\,000 \pm 500)$ K. The radius predicted for the scaled blackbody is 2.7 $R_\odot$ at the adopted distance of 2.0 kpc, from which a luminosity of 3550 $L_\odot$ can be derived. A similar exercise for the Kurucz atmospheres yields a radius of 2.3 $R_\odot$ and a stellar luminosity of 6300 $L_\odot$.

de Freitas Pacheco & Veliz (1987) derived a blackbody H I Zanstra temperature of 32 000 K. A comparison by Flower et al. (1984) of the stellar ultraviolet and nebular free–free radio continuum fluxes yielded a blackbody H I Zanstra temperature of 36 000 K, although they found that a 30 000-K blackbody better fitted their optical and UV dereddened stellar energy distribution.

8.2 Modelling strategy and results

Photoionization modelling of PNe is the best way to test the internal consistency of an empirical analysis. The Harrington photoionization code applied here (Harrington et al. 1982) assumes that the nebula can be represented by a hollow spherical shell which is ionized only by a central star, and sampled by 60 radial grid points.

The Kurucz model and blackbody luminosities and the distance were fixed at the values derived above. An *inner* nebular angular radius of 0.22 arcsec (approximately 5 pixels) was determined from the *HST* observations, and scaled to the adopted distance (2.0 kpc) to yield an inner radius of 0.0086 pc. The clumping and vacuum filling factors were varied so as to reproduce the dereddened Hβ flux. The electron density was kept constant throughout the PN, fixed at the empirically derived value, except in the case of the WR flux distribution, for which this value overestimated the Hβ flux even for extremely low values of the filling factor, a fact that was judged non-physical. In theory, such a high-density PN is likely to be optically thick, such that a correct modelling procedure should make sure that the model reaches far enough to include the edge of the Strömgren sphere. This is achieved by increasing the thickness of the PN shell until the PN recombines at the outer grid points. On the other hand, following this procedure would mean that the thickness of the ionized shell and the corresponding Hβ flux would be much larger than observed, a fact that cannot be compensated for by reducing the filling factor within sensible limits. We therefore used the observed values for the inner and outer radii and accepted an optically thin PN. A non-constant density profile was not attempted. The efforts of De Marco & Crowther (1999) on the PN M4-18 did not produce better results when a variable density profile was adopted. Additionally, for the compact PN SwSt 1 the lack of a high signal-to-noise ratio image means that the density profile cannot be constrained.

As a starting point we adopted the empirically derived abundances. Lines of oxygen and carbon were then fitted by changing their abundances. Carbon and oxygen are important coolants, and changing the abundances not only varies the line strengths, but also the nebular electron temperature. When a compromise was reached on the strength of these lines and the electron temperature, lines of sulphur, nitrogen and neon were fitted by varying their abundances. The abundances of other unobserved species were left at the mean PN value as determined by Kingsburgh & Barlow (1994) for a set of 80 southern PN, or at their solar values. When the ionization balance of the element in question is very different from the observations, it is arbitrary to decide which lines should be fitted and which should be ignored. In the case of sulphur, we used the strong [S III] line at 9532 Å, ignoring [S II] lines. For oxygen, we fitted a compromise of the [O II] lines $\lambda\lambda$3726,29 and λ7325, forsaking [O III] lines. For neon, the [Ne II] line at 12.8 μm was used, while for carbon a compromise between the C II] λ2326 and C III] λ1908 lines was used. We note, however, that because none of the stellar flux distributions reproduces the observations to an acceptable precision, we found it unnecessary to fit individual spectral line fluxes to high accuracy.

In Table 12 we compare the abundances determined from modelling with the empirical values, as well as the predicted line fluxes with the dereddened observations. None of the stellar atmospheres used reproduces the observed characteristics of SwSt 1's PN to an acceptable degree of accuracy. In the case of the WR flux distribution, we decided that lowering the electron density to about half the observed value was preferable to having an

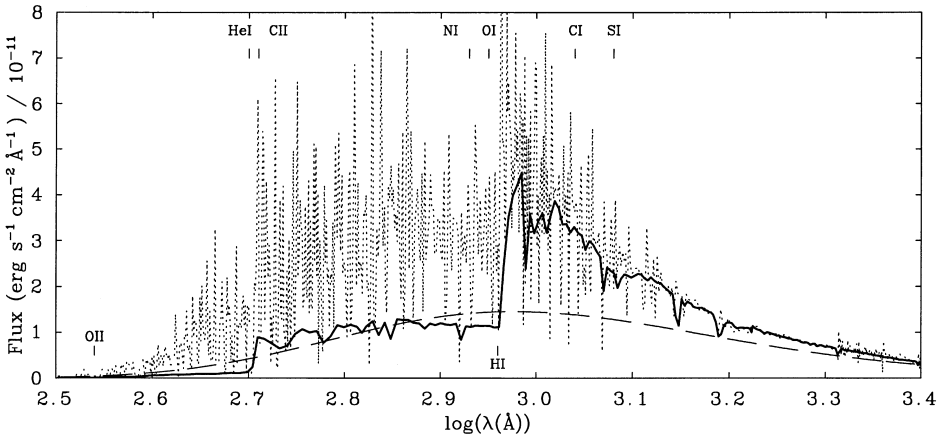

Figure 13. A comparison of the ISA-Wind line-blanketed non-LTE model atmosphere (dotted line) with the 30 300-K blackbody flux distribution (dashed line), and a 34 000-K, log(g) = 4.0 plane-parallel Kurucz model atmosphere (thick solid line). The H I, He I and other important ionization edges are marked.

extremely low filling factor (∼0.02, too low even if the PN is actually a ring as the *HST* image might suggest). With this value of the electron density, a more acceptable filling factor of 0.76 was needed to reproduce the Hβ flux. However, this implies an optically thin PN. The overall ionization balance is overestimated except that of sulphur, which is underestimated. Interestingly, a cooler WR stellar atmosphere also failed to reproduce the ionization balance. We tried to use the 35-kK model which reproduces most of the stellar spectral features except the C IV/CIII ionization balance (see Section 5.5). This model severely underestimates the nebular ionization balance, while at the same time having a similar problem with the Hβ flux and the filling factor, as outlined above. We therefore believe that the failure of the PN model is not due to the hot WR atmosphere.

The blackbody and Kurucz stellar flux distributions underestimate the ionization balance of carbon, but overestimate that of oxygen. They give mixed results in the case of neon and sulphur. With particular reference to oxygen, we point out that the [O III] lines used are extremely susceptible to small temperature changes; in particular, it appears that for central star effective temperatures above ∼38 kK the [O III] lines increase dramatically in flux (Miriam Peña, private communication). For these stellar flux distributions we were able to use the electron density determined from observations, although, once again, we had to accept an optically thin PN, so as to obtain a sensible value for the filling factor. An optically thin PN is, however, more in disagreement with an electron density of 31 600 cm^{-3}. The three stellar atmospheres are compared in Fig. 13.

The nebular mass implied by all the stellar flux distributions is very low compared to the canonical value of 0.3 M$_\odot$ for optically thin PN. As for the optical depth properties of this PN, it is unusual to have an optically thin PN with an electron density as high as we encountered. On the other hand, the fact that the Zanstra analysis returns values of the effective temperature lower than those determined with an ad hoc modelling of the stellar spectrum with a non-LTE code might suggest that the Hβ flux is not representative of the hard photon population, i.e., that the PN is indeed optically thin.

In conclusion, no matter the method chosen for the modelling effort, we have found no way of fitting the observed properties of this PN to a satisfactory accuracy. We take this to mean that the modelling tool being used is inadequate for the PN of SwSt 1. In particular, the simple shell geometry might be far from the truth of this young PN. Nebular modelling with our CMFGEN models atmosphere as input was not attempted. Overall, the two flux distributions compare reasonably well, with ISA-Wind harder far-UV flux being compensated by CMFGEN's higher effective temperature. CMFGEN would therefore not succeed in reproducing the [O III] lines.

9 SWST 1 BETWEEN 1895 AND 1993

The warm oxygen-rich dust revealed by the 10-μm silicate emission feature, and the high nebular density, indicate that SwSt 1 has recently made the transition from the AGB. This could indicate that the pulse that caused SwSt 1 to become H-deficient might have occurred in the last century, i.e., after it was first observed in 1895. Since variability of the stellar and nebular lines has been noted by Carlson & Henize (1979) and by de Freitas Pacheco & Veliz (1987), we decided to investigate the variability issue. Photographic spectra of SwSt1 were examined by taking a cut through a scan of the plate that appeared in the original paper. We then applied a rough wavelength calibration. Obviously, some fidelity is lost in this process, but the spectra are still useful qualitatively.

SwSt 1 was discovered to be an emission line star by James E. Keeler in 1895 (Fleming 1895). He reported Balmer lines in emission and compared the spectrum to that of η Car. Although we could not find his spectrum in the literature, we examined a scan from another plate taken in 1896 which shows only three emission lines (Hβ and [O III] $\lambda\lambda$4959,5007) superimposed on a stellar continuum. On the basis of this spectrum, SwSt 1 is referred to as P Cygni class by Fleming in her log-book. Cannon (1916), referring to these or similar spectra, also assigned SwSt 1 to the P Cygni class. These early spectra of SwSt 1 are very low-dispersion prism spectra. Although P Cygni profiles had already been recognized in other stars, it is doubtful that they could be resolved on these plates. It is more likely that SwSt 1 was classified as P Cygni on the basis of bright Balmer lines on top of a stellar continuum. Cannon (1921) mentions the presence of [O III] $\lambda\lambda$4959,5007 emission in SwSt 1. She notes that these lines are associated with gaseous nebulae (even though they were not identified until 1928).

Subsequently, SwSt 1 was observed spectroscopically on six distinct occasions: by Payne Gaposchkin & Gaposchkin (1938a,b, source spectra unknown); in 1940 by Swings & Struve (1940; in the range 3600–6680 Å at dispersions of 100 and 50 Å mm^{-1}); in 1942 by Swings & Struve (1943; 3600–5300 Å); in 1962 by

Carlson & Henize (1979; in the range 3700–6600 Å at a dispersion of 177 Å mm^{-1} blue-ward of 5000 Å and 94 Å mm^{-1} red-ward of 5000 Å); by Aller (1977, although the date of the spectrum is not indicated; the range of the observations is 5000–8500 Å); in 1976 by Flower et al. (1984; in the range 4260–6710 Å at a resolution of 7 Å); in 1985 by de Freitas Pacheco & Veliz (1987; in the range 3600–6930 Å at resolutions of 6.5 and 0.5 Å); in by Leuenhagen & Hamann (1998; in the ranges 3800–5000 Å and 5800–6700 Å at a resolution of 1 Å) and by us in 1993 (in the range 3700–5400 Å at a resolution of 0.15 Å, and in the range 5400–9200 Å at a resolution of 0.35 Å).

Two trends since 1940 have been suggested in the literature: a weakening of the stellar wind lines and an increasing degree of ionization of both the stellar wind and the PN. The former trend was pointed out by Carlson & Henize (1979), who noted the possible disappearance of several weak stellar O III and C III lines between 1940 and 1962, along with the appearance of [Fe II] and [Fe III] lines. They also reported the diminution of P Cygni profiles, from a total of 10 lines (as counted by Swings & Struve 1940) to four lines, finally concluding that the wind's density and mass-loss rate must have decreased between the two observations.

We looked at the plate reproductions in the original 1940 and 1962 papers, and we also took a cut along the spectral direction of scanned-in versions. To within the precision allowed by our method, we notice no obvious change. It is possible that weak P Cygni profiles were apparent to Swings & Struve in the original plate material, and that these features had become weaker by 1962 when observed by Carlson & Henize. One might, in fact, expect the star to have gradually lost its hydrogen during its early post-AGB phase. We have no reason to doubt the claim by Swings & Struve that Hγ and Hϵ had P Cygni profiles but not Hα, Hβ or Hδ. However, we would like to point out that Hα is generally the first line to develop an emission component and a P Cygni profile in the presence of a wind. Looking at the 1940 spectrum, we do notice, however, that the stellar continuum is extremely irregular, while in 1960 it is much smoother. Such irregularity, combined with a variety of emission lines, could have given the impression of troughs, which could in turn have been interpreted as P Cygni.

The claim of Carlson & Henize (1979) that [Fe II] and [Fe III] emission appeared sometime between 1940 and 1962 is also somewhat suspect, since [Fe II] emission was already reported previous to 1940, by Payne Gaposchkin in 1938. However, by far the most misleading statement about variability reported in the literature is the claim of Carlson & Henize (1979) that the C III λ5696 and C IV $\lambda\lambda$5801,12 lines are absent from the 1962 spectrum of SwSt 1. These lines are prominent in the spectrum of Swings & Struve (1942) and also in our own spectrum. The Carlson & Henize (1979) 1962 spectrum longward of 5000 Å comes from a very weakly exposed plate compared to their other material. On that plate only the strong nebular [N II] λ6583 line and Hα are visible, with He I λ5876 described as being barely visible. The C III λ5696 and C IV $\lambda\lambda$5801,12 lines are several times weaker than λ5876 in our spectrum, and would be well below their plate limit. On this basis, the claim that C III λ5696 and C IV $\lambda\lambda$5801,12 are not present in 1962 can be dismissed.

The only spectral change which seems real, comes from the spectroscopy of Aller (1977). From his fig. 4 we see that C IV λ5470 is much stronger and broader than the neighbouring He II/[Fe III] blend at 5411 Å. In the spectrum presented here, the strength of the two lines is comparable. However, the C IV lines at 5801 and 5812 Å are not stronger in Aller's spectrum, so that no consistent trend is noticed.

de Freitas Pacheco & Veliz (1987) advocate a second trend, increasing ionization of both the stellar wind and the PN. They were not able to see any nebular [Fe II] lines in their spectra despite the far superior resolution of their data compared with earlier spectra, and noticed instead weak lines which they attributed to [Fe IV]. Although de Freitas Pacheco & Veliz do not show any of the spectral regions containing [Fe II] lines, from the quality of their published spectroscopy we suggest that they would not have been able to observe the weak [Fe II] lines detectable in our 1993 spectrum. However, since the 1938 and 1962 spectroscopy is likely to have been of poorer signal-to-noise ratio than their 1985 data, we conclude that [Fe II] lines have indeed weakened, and that the fact that we do observe them in the 1993 spectrum is only because of our higher resolution. Based on the weakening of the nebular [Fe II] lines, we conclude that the PN *might* have increased its level of ionization, although we attach a large uncertainty to this statement. However, the argument that the stellar wind has increased in ionization is based on the erroneous claim by Carlson & Henize (1979) of the absence of the C IV lines at 5801 and 5812 Å in 1962.

In conclusion, the arguments for a significant evolution of the spectrum of SwSt 1 in the last century are weak. The PN might have increased its level of ionization slightly, and there might have been some variability in the stellar wind spectrum, but nothing major has happened to this central star in the last 60 years and possibly in the 110 years since it was first observed.

10 DISCUSSION

From the properties derived for SwSt 1 we can state the following. Although the possible distance range of 2–4 kpc is large, even at a distance of 2 kpc the stellar luminosity implied by the models points to a central star mass at the high end of the PN distribution. As we have seen, the distance issue poses a significant obstacle and does not allow us to determine the stellar and nebular parameters with sufficient accuracy to establish relationships between different objects. Better parallaxes, or expansion distances are the only way to get around the problem. Another way would be to find [WCL] stars in the Magellanic Clouds and use those to characterize the sample. A wide-field survey would be needed, sensitive enough to detect emission-line stars with equivalent widths of the order of a few Ångströms and 8-m-class telescope follow-up spectroscopy.

The stellar analysis indicates a hotter star than previously implied (Leuenhagen & Hamann 1998), and more in conformity with the [WC9] spectral classification. The weakness of SwSt 1's stellar lines can be attributed to a relatively low mass-loss rate, although the derived value of $1.90 \times 10^{-7}\,M_{\odot}\,yr^{-1}$ should be quoted with care because of its distance dependence. Also noteworthy is the stellar wind oxygen abundance. This determination is reliant on a single line of O III, but no other lines exist in the available spectral range which contradict this determination. The new stellar evolutionary calculations of Herwig (2000) show that the oxygen abundance of models which account for convective overshoot (which begin to account for the severe hydrogen deficiency of WR central stars) should have a 10–20 per cent oxygen mass fraction. This is in agreement with our oxygen determination. Additionally, the C/O mass ratio is in the range 2–4 (depending on what modelling effort we rely on), showing third dredge-up enrichment. This is not dissimilar from the values obtained for the [WC10] stars CPD $-$ 56°8032 and He 2-113 of 3.7 and 4.1, respectively.

The PN of SwSt 1 is compact and of high density. It is likely to

be stratified as indicated by the *HST* Hβ image being larger than the [O III] image and by the lines from higher ionization stages being narrower. The nitrogen abundance is not particularly high, which is surprising if the central star is as massive as is implied by other parameters. Its other nebular abundances are not particularly unusual when compared to the mean values obtained by Kingsburgh & Barlow (1994) for non-Type I PNe. We confirm again that the C/O ratio is smaller than unity (0.7 by mass), indicating an O-rich PN. This is interesting in view of the stellar C/O ratio of 2–4, indicating active dredge-up between when the nebular material was ejected the present time. A study of the C/O variation as a function of distance from the star is underway for SwSt 1, CPD − 56°5682 and He 2-113 (De Marco et al., in preparation).

The PN neutral envelope presents a fair amount of atomic (e.g., sodium; Dinerstein et al. 1995), and only weak molecular H_2 emission is observed in our SOFI spectrum. We find that modelling this PN with a simple shell geometry and a smooth electron density fails no matter what stellar flux distribution is used. For a distance of 2 kpc, our best-fitting model has a luminosity of 8900 $L_\odot$, significantly higher than the reradiated IR dust luminosity of 1450 $L_\odot$, implying that either the dust shell does not absorb and reradiate the stellar luminosity, or else that our stellar model is not valid. On this line we also note that the relatively low N/H PN abundance ratio does not point to a particularly massive central star. Additionally, if wind strength correlates with luminosity, as is the case for radiation-driven winds, the weakness of the wind would also tend to point to a lower mass.

After carefully assessing the spectral variability reported in the literature by going back to the original publications and spectral plates, we cannot fully corroborate any of the changes reported in the spectrum of SwSt 1. From this we conclude that the star has not changed significantly over the past 100 years. Certainly we have not caught SwSt 1 before the pulse that transformed it into a hydrogen-deficient star. The dynamical time-scale of 150–330 yr refers to the edge of the ionized PN, although for such a high-density object we might expect this to be only a lower limit, since the PN material might not be fully ionized.

ACKNOWLEDGMENTS

OD acknowledges support through PPARC grant PPA/G/S/1997/00780 while at University College London. GCC and OD were supported by NASA ATP grant NAG5/9203. OD gratefully acknowledges the financial support of Janet Jeppson Asimov. We thank Arlo Landolt for obtaining optical photometry of SwSt 1, while Martin Cohen and Falk Herwig are thanked for many useful discussions. We are also grateful to John Hillier for making his modelling code, CMFGEN, available to us, and for the useful comments he made as the paper's referee. This work is based, in part, on observations collected at the European Southern Observatory, La Silla, Chile (Proposal No. 63.H−0683).

REFERENCES

Aaquist O. B., Kwok S., 1990, A&AS, 84, 229
Acker A., Stenholm B., Tylenda R., 1989, A&AS, 77, 487
Acker A., Fresneau A., Pottasch S. R., Jasniewicz G., 1998, A&A, 337, 253
Aitken D. K., Roche P. F., 1982, MNRAS, 200, 217
Allen D. A., Glass I. S., 1974, MNRAS, 167, 337
Aller L. H., 1977, J. R. Astron. Soc. Can., 71, 67
Balick B., Rugers M., Terzian Y., Chengalur J. N., 1993, ApJ, 411, 778
Balick B., 1994, ApJ, 424, 800
Barlow M. J., 1997, Ap&SS, 251, 15
Cahn J. H., Kaler J. B., Stanghellini L., 1992, A&AS, 94, 399
Cannon A. J., 1916, Harvard Annals, 76
Cannon A. J., 1921, Harvard Circular, 224
Carlson E. D., Henize K. G., 1979, Vistas Astron., 23, 213
Cohen M., 1975, MNRAS, 173, 489
Cohen M., 2001, Ap&SS, 275, 103
Cohen M., Barlow M. J., 1974, ApJ, 193, 401
Cohen M. et al., 1999, ApJ, 513, L135
Crowther P. A., De Marco O., Barlow M. J., 1998, MNRAS, 296, 367
Crowther P. A. et al., 1999, A&A, 350, 1007
de Freitas Pacheco J. A., Veliz J. G., 1987, MNRAS, 227, 773
de Koter A., Schmutz W., Lamers H. J. G. L. M., 1993, A&A, 277, 561
de Koter A., Heap S. R., Hubeny I., 1997, ApJ, 477, 792
De Marco O., Barlow M. J., Storey P. J., 1997, MNRAS, 292, 86 (DBS97)
De Marco O., 2001, Ap&SS, in press
De Marco O., Barlow M. J., 2001, Ap&SS, 275, 53
De Marco O., Crowther P. A., 1998, MNRAS, 296, 419
De Marco O., Crowther P. A., 1999, MNRAS, 306, 931
De Marco O. et al., 2000, A&A, 358, 187
De Marco O., Barlow M. J., Cohen M., 2001, poster at Am. Astron. Soc. Meeting 197, 114.02
Dessart L. et al., 2000, MNRAS, 315, 407
Dinerstein H. L., Sneden C., Uglum J., 1995, ApJ, 447, 262
Fleming W. P., 1895, ApJ, 2, 354
Flower D. R., Goharji A., Cohen M., 1984, MNRAS, 206, 293
Goodrich R. W., Dahari O., 1985, ApJ, 289, 342
Gorny S. K., Stasinska G., 1995, A&A, 303, 893
Hamann W.-R., Koesterke L., 2000, A&A, 360, 647
Harrington J. P., Seaton M. J., Adams S., Lutz J. H., 1982, MNRAS, 199, 517
Herwig F., 1999, A&A, 349, L5
Herwig F., 2000, A&A, 360, 952
Hillier D. J., Miller D. L., 1998, ApJ, 496, 407
Hillier D. J., Miller D. L., 1999, ApJ, 519, 354
Howarth I. D., 1983, MNRAS, 203, 301
Howarth I. D., Murray J., Mills D., Berry D. S., 1995, Starlink User Note 50.16, Rutherford Appleton Laboratory
Huggins P. J., Bachiller R., Cox P., Forveille T., 1996, A&A, 315, 284
Iben I., Jr, Kaler J. B., Truran J. W., Renzini A., 1983, ApJ, 264, 605
Jones A. et al., 1999, Observatory, 119, 1149
Kastner J. H., Weintraub D. A., Gatley I., Merrill K. M., Probst R. G., 1996, ApJ, 462, 777
Kaufman V., Sugar J., 1986, J. Phys. Chem. Ref. Data, 15, 321
Keyes C. D., Aller L. H., Feibelman W. A., 1990, PASP, 102, 59
Kingsburgh R. L., Barlow M. J., 1992, MNRAS, 257, 317
Kingsburgh R. L., Barlow M. J., 1994, MNRAS, 271, 257
Kurucz R. L., 1991, in Crivellari L., Hubeny I., Hummer D. G., eds, Stellar Atmospheres Beyond Classical Models, Proceedings of the Advanced Research Workshop, Trieste, Italy. Reidel, Dordrecht, p. 441
Kwok S., Purton C. R., Keenan D. W., 1981, ApJ, 250, 232
Landolt A. U., 1992, AJ, 104, 340
Leuenhagen U., Hamann W.-R., 1998, A&A, 330, 265
Leuenhagen U., Hamann W.-R., Jeffery C. S., 1996, A&A, 312, 167
Mathis J. S., 1994, ApJ, 422, 176
Milne D. K., Aller L. H., 1975, A&A, 38, 183
Milne D. K., Aller L. H., 1982, A&AS, 50, 209
Oke J. B., 1990, AJ, 99, 1621
Payne Gaposchkin C. H., Gaposchkin S., 1938a, QB835.G3
Payne Gaposchkin C. H., Gaposchkin S., 1938b, Ann. Astrophys., 1, 430
Perek L., 1971, Bull. Astron. Inst. Czech., 22, 103
Perek L., Kohotek L., 1967, Catalogue of Galactic Planetary Nebulae. Czechoslovakian Academy of Science, Prague
Pottasch S. R., 1996, Ap&SS, 238, 17
Prinja R. K., Barlow M. J., Howarth I. D., 1990, ApJ, 361, 607
Schmutz W., 1997, A&A, 321, 268

Schmutz W., 1998, in Howarth I., ed., ASP Conf. Ser. Vol. 131, Boulder-Munich II: Properties of Hot, Luminous Stars. Astron. Soc. Pac., San Francisco, p. 119
Schmutz W. et al., 1991, ApJ, 372, 664
Schneider S. E., Terzian Y., Purgathofer A., Perinotto M., 1983, ApJS, 52, 399
Seaton M. J., 1995, The Opacity Project, Volume 1. Institute of Physics Publishing, Bristol, ISBN 0-7503-0288-7
Shortridge K. et al., 1999, Starlink User Note 86.17, Rutherford Appleton Laboratory
Smith L. F., 1968, MNRAS, 140, 409
Storey P. J., Hummer D. G., 1995, MNRAS, 272, 41
Swings P., Struve O., 1940, Proc. Nat. Acad. Sci., 26, 454
Swings P., Struve O., 1943, ApJ, 97, 194
Szczerba R., Gorny S. K., Stasinska G., Sidmiak N., Tylenda R., 2001, Ap&SS, 275, 113
Tylenda R., Acker A., Stenholm B., 1993, A&AS, 102, 595
van de Steene G. C., Zijlstra A. A., 1994, A&AS, 108, 485
van der Hucht K. A., Conti P. S., Lundstron I., Stenholm B., 1981, Space Sci. Rev., 28, 227
van der Steene G. C., Zijlstra A. A., 1994, A&AS, 108, 485
Vassiliadis E., Wood P. R., 1994, ApJS, 92, 125
Waters L. B. F. M. et al., 1998, A&A, 331, 61L
Zhang C. Y., 1993, ApJ, 410, 239
Zahng C. Y., 1995, ApJS, 98, 659
Zhang C. Y., Kwok S., 1991, A&A, 250, 179
Zuckerman B., Gatley I., 1988, ApJ, 324, 501

APPENDIX A: THE NEUTRAL ENVELOPE OF SWST 1

The Na I D lines in the spectrum of SwSt 1 shown in Fig. 1 indicate a complex neutral envelope structure. Below we study this complex line system and compare our findings to those of Dinerstein et al. (1995).

The Na I D line negative LSR radial velocity troughs in the spectrum of SwSt 1 are unlikely to be of interstellar origin, since the Galactic radial velocity curve in the direction of SwSt 1 is positive (Fig. 1c). It is therefore likely that these components arise from a neutral envelope enclosing the ionized PN. As such they can be a good tracer of velocity components. We identified two components per line, with radial velocities at (-78 ± 5) and $(-38 \pm 2)\,\mathrm{km\,s^{-1}}$ (Fig. 1b). If corrected for the heliocentric radial velocity of the nebula, the Na I D line emission components lie at $(0 \pm 4)\,\mathrm{km\,s^{-1}}$, while the two troughs are measured to be at (-70 ± 5) and $(-28 \pm 2)\,\mathrm{km\,s^{-1}}$. The nebular expansion velocity determined in Section 3.2 is $(20 \pm 1)\,\mathrm{km\,s^{-1}}$. Hence we would expect absorption components of the Na D lines associated with the ionized nebula to be found at a heliocentric radial velocity of about $-20\,\mathrm{km\,s^{-1}}$. The trough associated with the first component is at about $-28\,\mathrm{km\,s^{-1}}$, $8\,\mathrm{km\,s^{-1}}$ more negative than expected, although this discrepancy can be almost justified by the relative uncertainties. The component at $-70\,\mathrm{km\,s^{-1}}$ then has to be explained by assuming that SwSt 1's PN has a neutral velocity component moving at a higher velocity than the ionized 'shell' measured by the Balmer lines. For the [WC10] stars CPD $-56°8032$ and He 2–113 (DBS97) there is a correspondence between the high-velocity components of the Na I D line troughs and the shape of the emission lines of [O I]. The same comparison in SwSt 1 reveals that fitting the [O I] lines with two Gaussians (of which one is forced to have a FWHM $= 40\,\mathrm{km\,s^{-1}}$) cannot encompass components with FWHM larger than $60\,\mathrm{km\,s^{-1}}$. This could explain a Na I D line component at about $-30\,\mathrm{km\,s^{-1}}$ (like the observed component at $-28\,\mathrm{km\,s^{-1}}$) but not the trough observed at $-70\,\mathrm{km\,s^{-1}}$. In conclusion, the absorbing sodium must be associated with a different part of the nebula from the collisionally excited neutral oxygen.

Dinerstein et al. (1995) also found evidence for circumstellar sodium around SwSt 1. They measured the emission component of the Na D lines to be at $-7\,\mathrm{km\,s^{-1}}$, while they determined the absorption component to be at $-27\,\mathrm{km\,s^{-1}}$ (where their measurements were corrected for a heliocentric nebular radial velocity of $-20\,\mathrm{km\,s^{-1}}$). These correspond within the uncertainties to our emission component at $0\,\mathrm{km\,s^{-1}}$ and absorption component at $-28\,\mathrm{km\,s^{-1}}$. They did not find a double absorption as we do, and indeed their fig. 2 is significantly different from our Fig. 1(a), although their claimed resolution (0.20 Å) is similar to our own. It is not possible at present to resolve this discrepancy. However, they did mention the possibility of the existence of higher velocity components in the PN envelope, and they compared this effect to the fast low-ionization outflows (FLIERs) described by Balick et al. (1993) and Balick (1994).

APPENDIX B: THE OPTICAL AND NEAR-IR SPECTRA OF SWST 1

In this appendix we present the UCL echelle spectrum of SwSt 1 obtained at the Anglo-Australian Telescope in 1993 May (Figs B1–B5), as well as our near-IR NTT SOFI spectrum (Fig. B6; details of the data acquisition and reduction are presented in Section 2). Due to the strength of the nebular lines compared to the stellar lines, we present the rectified optical spectrum on a log scale.

In Table B1 we present a list of the lines we identified in the optical spectrum of SwSt 1. In column 4 we indicate the origin of the line (*s* for stellar, *n* for nebular, *is* for interstellar), while in column 5 we list the initials of the authors who have identified those lines in the past. A discussion of the stellar and nebular components of SwSt 1's optical spectrum has been presented in Sections 5.1 and 6.1.

The near-IR SOFI spectrum is dominated by strong nebular emission lines of H I (e.g., Pβ, Brγ) and He I (1.083 and 2.058 μm), plus [S III] 9530 Å (Table B2). As reported in Section 2.1, we have detected H_2 [at 2.1218 μm ($v = 1$–0, S(1)] for the first time from this young PN.

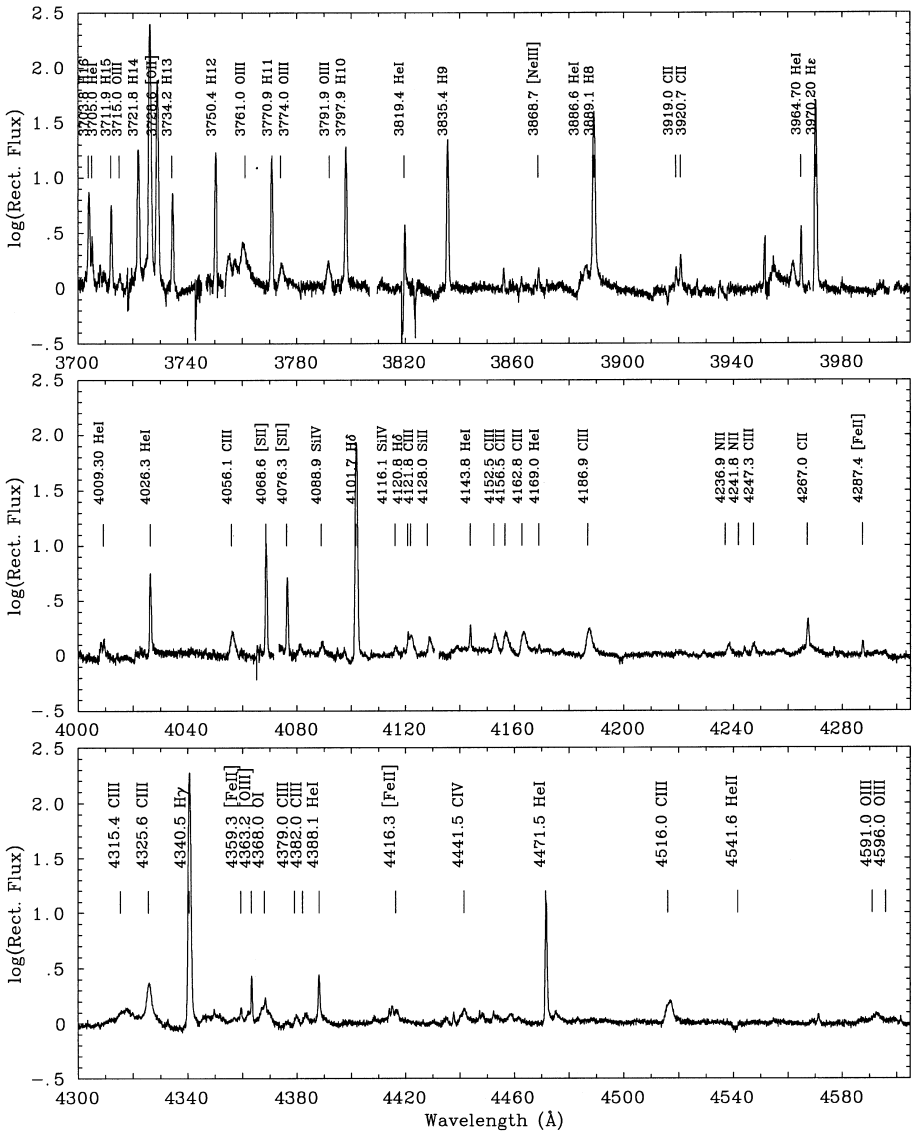

Figure B1. The AAT spectrum of SwSt 1 between 3700 and 4605 Å.

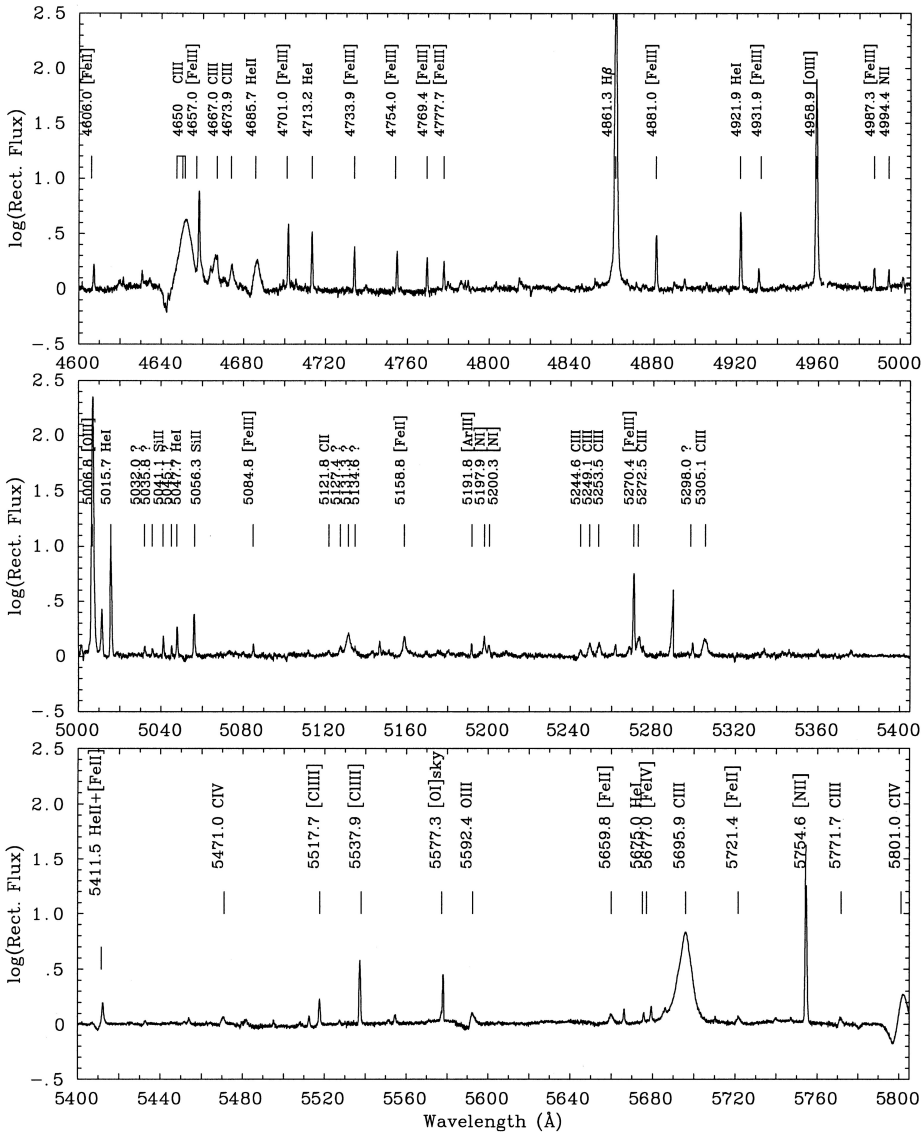

Figure B2. The AAT spectrum of SwSt 1 between 4600 and 5805 Å.

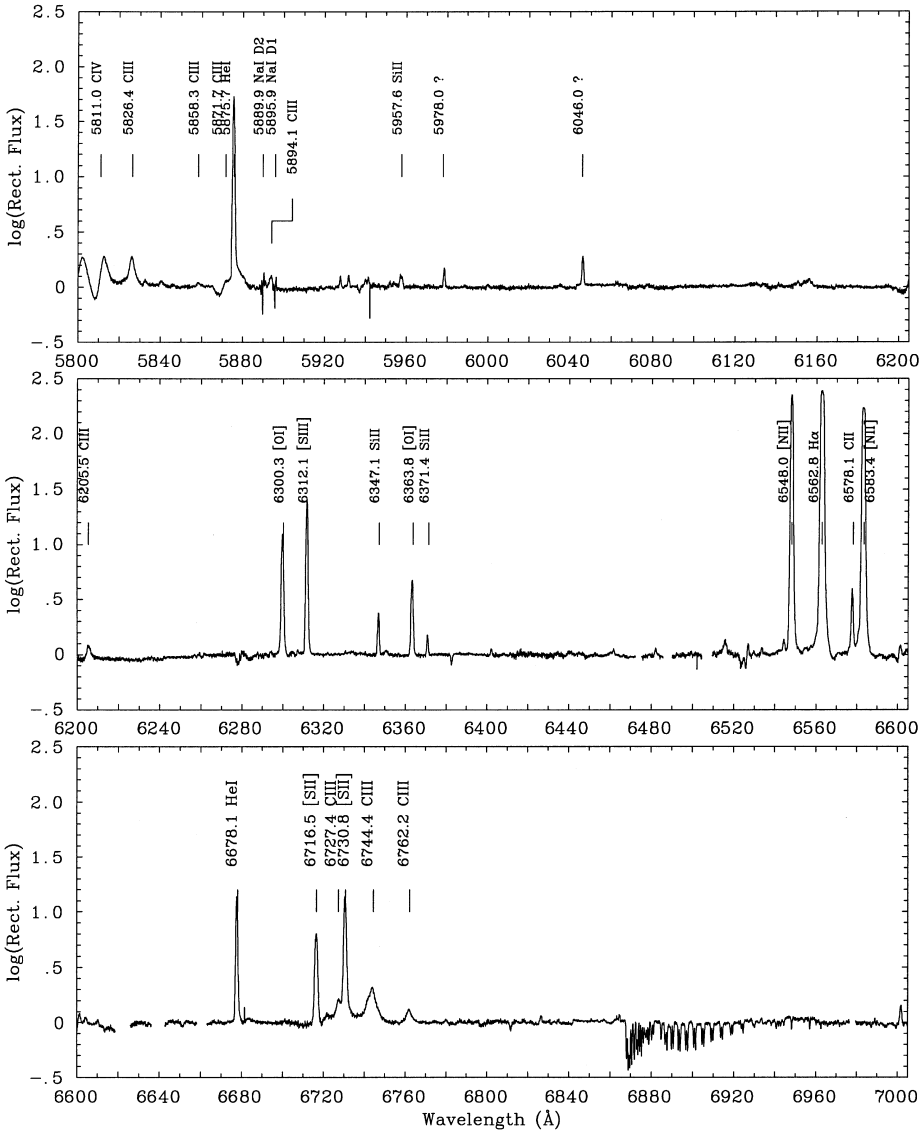

Figure B3. The AAT spectrum of SwSt 1 between 5800 and 7005 Å.

Table B1. Lines identified in the spectrum of SwSt 1 between 3700 and 9700 Å.

Ion	Wavelength (Å)	Multiplet No.	Origin	Comments
H16	3703.8		n	SS,CH
He I	3705.0	25	n	CH
H15	3711.9		n	SS,CH
O III	3715.0	14	s	SS
H14	3721.8		n	SS,CH,dFV
[O II]	3726.2	1F	n	SS,CH,dFV
[O II]	3728.9	1F	n	SS,CH,dFV
H13	3734.2		n	SS,CH
H12	3750.4		n	SS,CH
O III	3761.0	30	s	SS
H11	3770.9		n	SS,CH,dFV
O III	3774.0	2	s	
O III	3791.3	2	s	
O III	3791.9	2	s	SS
H10	3797.9		n	SS,CH,dFV
He I	3819.4	22	n	SS,CH
H9	3835.4		n	SS,CH,dFV
[Ne III]	3967.7		n	
He I	3888.7	2	n	SS
H8	3889.1		n	SS,CH,dFV
C II	3919.0	4	n	CH
C II	3920.7	4	n	CH
He I	3964.7	5	n	SS,CH
Hϵ	3970.2		n	SS,CH,dFV
He I	4009.4	55	n	
He I	4026.3	18	n	SS,CH
C III	4056.1	24	s	SS,CH
[S II]	4068.6	1F	n	SS,CH,dFV
[S II]	4076.3	1F	n	SS,CH,dFV
Hδ	4101.7		n	SS,CH,dFV
He I	4120.8	16	n	
C III	4121.8	17	s	
Si II	4128.0	3	s	CH
Si II	4130.9	3	s	
N II	4136.9		s/n?	
He I	4143.8	53	n	SS,CH
C III	4152.5	21	s	
C III	4156.5	21	s	SS
C III	4162.8	21	s	
He I	4169.0	52	n	
C III	4186.9	18	s	SS,CH
N II	4241.8		s/n?	
C III	4247.3	11	s	
C II	4267.0	6	n+s	CH,dFV
[Fe II]	4287.4	7F	n	CH
C III	4315.4	48	s	
C III	4325.6	7	s	CH
Hγ	4340.5		n	SS,CH,dFV
[Fe II]	4359.3	7F	n	CH
[O III]	4363.2	2F	n	SS,CH,dFV
O I	4368.0		n	dFV
C III	4379.0	14	s	
C III	4382.0	14	s	
He I	4388.1	51	n	SS,dFV,CH
[Fe II]	4416.3	6F	n	CH
C IV	4441.5		s	
C III	4650.3	1	s	SS,CH
C III	4651.5	1	s	SS,CH
[Fe III]	4657.0	3F	n	dFV,CH
C III	4663.6	5	s	
C III	4667.0	5	s	SS
C III	4673.9	5	s	
He II	4685.7	3-4	s	SS,CH
[Fe III]	4701.0	3F	n	CH,dFV
He I	4713.2	12	n	CH,dFV
[Fe III]	4733.9	3F	n	CH,dFV
[Fe III]	4754.0	3F	n	dFV
[Fe III]	4769.4	3F	n	
[Fe III]	4777.7	3F	n	

Table B1 – *continued*

Ion	Wavelength (Å)	Multiplet No.	Origin	Comments
Hβ	4861.3		n	SS,CH,dFV
[Fe III]	4881.0	2F	n	
He I	4921.9	48	n	CH,dFV
[Fe III]	4930.5	1F	n	
[O III]	4958.9	1F	n	SS,CH,dFV
[Fe III]	4987.3		n	
N II]	4994.4		s/n	
[O III]	5006.8	1F	n	SS,CH,dFV
He I	5015.7	4	n	dFV
?	5032.0			
?	5035.8			
?	5041.1			
He I	5047.7	47	n	
Si II	5056.0	5	n?	
[Fe III]	5084.8			
C II	5121.8			
?	5130.8		s	
[Fe II]	5158.8	19F	n	
[Ar III]	5191.8	3F	n	
[N I]	5197.9	1F	n	
[N I]	5200.3	1F	n	
C III	5244.6	4	s	
C III	5249.1	23	s	
C III	5253.5	4	s	
[Fe III]	5270.0	1F	n	dFV
C III	5272.5	4	s	
?	5298.0			
C III	5305.1	46	s	
He II	5411.5	4-7	s	
C IV	5471.0		s	
[Cl III]	5517.7	1F	n	dFV
[Cl III]	5537.9	1F	n	dFV
[O I]	5577.3	3F	n	sky
OIII	5592.4	5	s	
[Fe II]	5659.8		n	
He I	5675.0		n	
C III	5695.9	12	s	SS
[Fe II]	5721.4	33F	n	
[N II]	5754.6	3F	n	SS,dFV
C III	5771.7		s	
C IV	5801.3	1	s	SS,dFV
C IV	5812.0	1	s	dFV
C III	5826.4	22	s	
C III	5857.9	20	s	
C III	5871.6	20	s	
He I	5875.7	11	n	SS,CH,dFV
Na I D2	5889.9		n+is	
C III	5894.2	20	s	
Na I D1	5895.9		n+is	
Si II	5957.6	4	s/n?	
C III	6205.5	17	s	
[O I]	6300.3	1F	n	SS,dFV
[S III]	6312.1	3F	n	SS,dFV
[O I]	6363.8	1F	n	dFV
[N II]	6548.0	1F	n	SS,CH,dFV
Hα	6562.8		n	SS,CH,dFV
Si II	6347.1	2	n/s?	
Si II	6371.4	2	n/s?	
C II	6578.1	2	n	
[N II]	6583.4	1F	n	SS,CH,dFV
He I	6678.1		n	SS,dFV
[S II]	6716.5	2F	n	dFV
C III	6727.4	3	s	
[S II]	6730.8	2F	n	dFV
C III	6744.4	3	s	
C III	6762.2	3	s	
C III	7037.2	6.01	s	
He I	7065.7	10	n	
[Ar III]	7135.8	1F	n	
C II	7231.3	3	n	

Table B1 – *continued*

Ion	Wavelength (Å)	Multiplet No.	Origin	Comments
C II	7236.4	3	n	
He I	7281.3	45	n	
[O II]	7319.9	2F	n	
[O II]	7330.1	2F	n	
C III	7486.5	41	s	
C III	7586.4	2.02	s	
C III	7707.4	10.01	s	
[Ar III]	7751.1	1F	n	
C III	7771.8	26	s	
C III	7780.4	26	s	
C III	7796.0	26	s	
C III	8196.2	43	s	
H3-20	8392.4		n	
H3-19	8413.3		n	
H3-18	8438.0		n	
H3-17	8467.3		n	
[Cl III]	8500.0		n	
C III	8500.3	1.01	s	
H3-16	8502.5		n	
H3-15	8545.4		n	
[Cl II]	8578.7		n	
H3-14	8598.4		n	
[Fe II]	8617.0		n	
H3-13	8665.1		n	
H3-12	8750.5		n	
H3-11	8862.7		n	
H3-10	9014.9		n	
[S III]	9068.9	1F	n	
H3-9	9229.0		n	
[S III]	9531.0	1F	n	

SS = Swings & Struve 1940; range 3600–6680 Å; dispersion 100 and 50 Å mm^{-1}.
CH = Carlson & Henize 1979; observations taken in 1962, range 3700–6600 Å, resolution 177 Å mm^{-1} up to 5000 Å, 94 Å mm^{-1} thereafter.
dFV = de Freitas Pacheco & Veliz 1984; range 3600–5900 Å, resolution 6.5 and 0.5 Å; NB some lines observed by them might be missing.

Table B2. Principal near-IR line fluxes, F_λ, obtained from NTT-SOFI observations of SwSt 1, together with dereddened fluxes relative to $I(\mathrm{H}\beta) = 1.50 \times 10^{-10}\,\mathrm{erg\,cm^{-2}}s^{-1}$, assuming $E(B-V) = 0.46$ mag. Uncertain values are given in parenthesis (due to poor atmospheric transmission).

λ_{obs} (μm)	Identification	λ_{lab} (μm)	F_λ (erg cm^{-1} s^{-1})	$100 \times I_\lambda$ /I(Hβ)
0.954	[SIII]	0.953	7.56×10^{-11}	90.7
0.971	CIII(3p-3d)	0.971	2.30×10^{-12}	2.7
1.005	Pδ	1.005	4.86×10^{-12}	5.6
1.033			1.24×10^{-12}	1.3
1.084	HeI(2s-2p)	1.083	5.69×10^{-11}	60.8
1.094	Pγ	1.094	8.46×10^{-12}	9.0
1.198	CIII(4s-4p)	1.198	3.7×10^{-13}	0.4
1.282	Pβ	1.282	1.56×10^{-11}	14.8
1.317			2.6×10^{-13}	0.2
1.520	HI(4-20)	1.519	1.4×10^{-13}	0.1
1.527	HI(4-19)	1.526	1.5×10^{-13}	0.1
1.535	HI(4-18)	1.534	2.3×10^{-13}	0.2
1.544	HI(4-17)	1.544	2.2×10^{-13}	0.2
1.556	HI(4-16)	1.556	2.5×10^{-13}	0.2
1.571	HI(4-15)	1.570	3.3×10^{-13}	0.3
1.589	HI(4-14)	1.588	4.1×10^{-13}	0.3
1.612	HI(4-13)	1.611	4.4×10^{-13}	0.4
1.641	HI(4-12)	1.641	6.5×10^{-13}	0.5
1.681	HI(4-11)	1.681	8.0×10^{-13}	0.7
1.701	HeI(3p-4d)	1.700	1.5×10^{-13}	0.1
1.737	Brζ	1.736	9.1×10^{-13}	0.7
1.818	Brϵ	1.817	3.5×10^{-12}	2.8
1.875	Pα	1.875	(1.78×10^{-11})	(14.0)
1.945	Brδ	1.945	1.9×10^{-12}	1.5
2.058	HeI(2s-2p)	2.058	1.4×10^{-12}	1.0
2.122	H_2(0-1, S(1))	2.122	1.5×10^{-13}	0.1
2.166	Brγ	2.166	3.2×10^{-12}	2.4

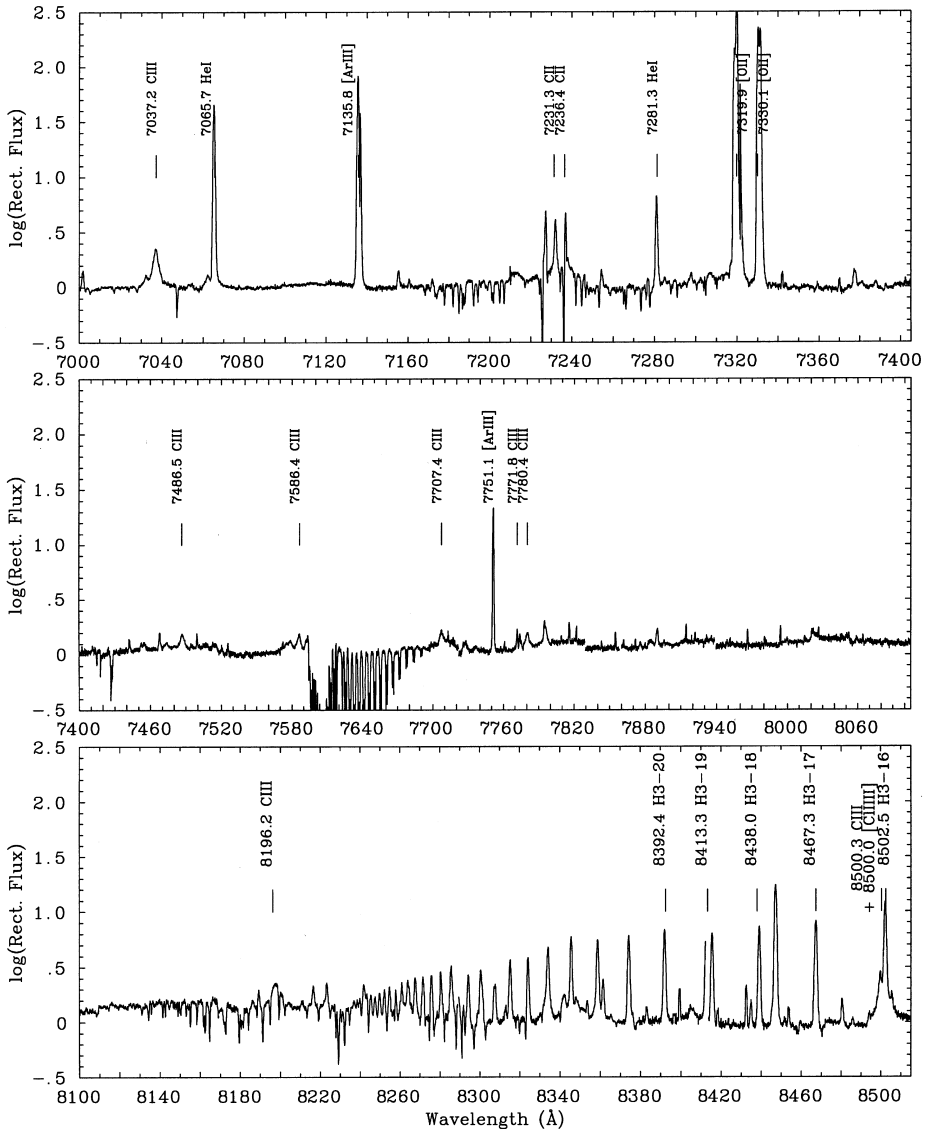

Figure B4. The AAT spectrum of SwSt 1 between 7000 and 8515 Å.

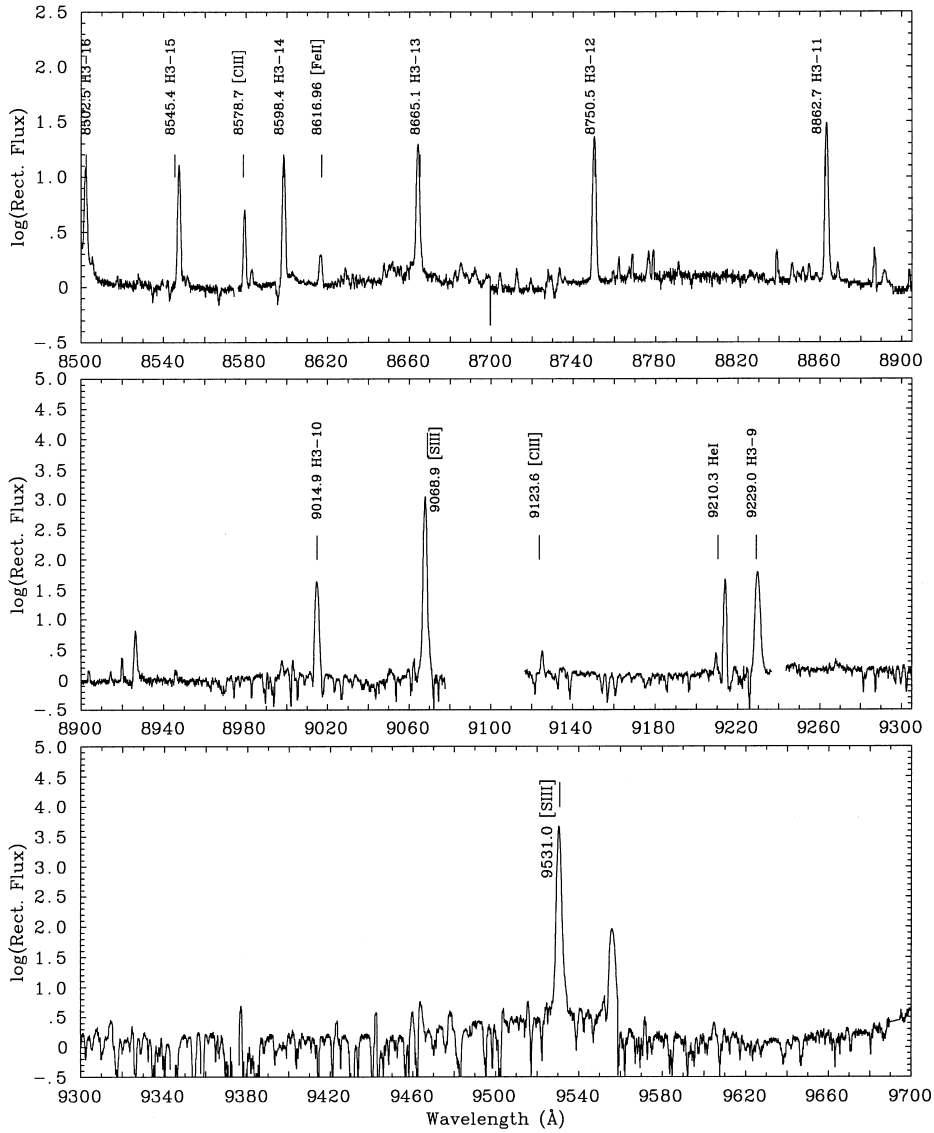

Figure B5. The AAT spectrum of SwSt 1 between 8500 and 9700 Å.

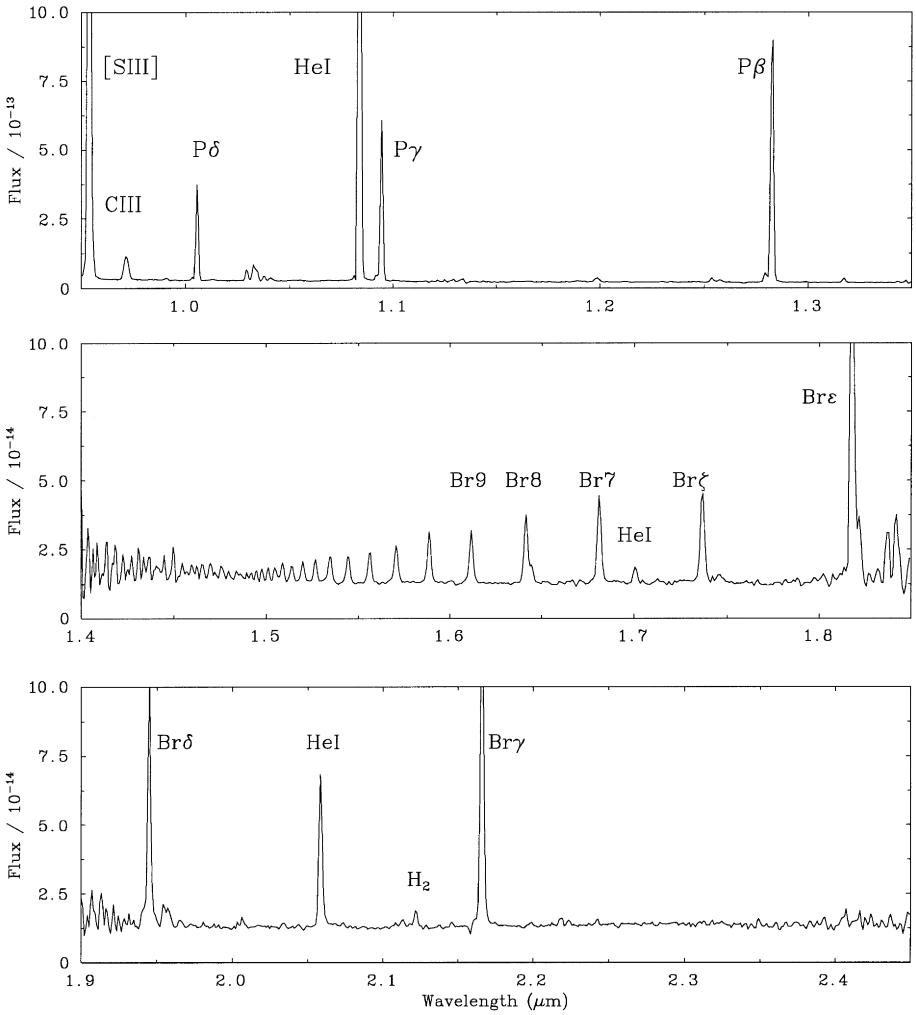

Figure B6. The SOFI spectrum of SwSt 1.

This paper has been typeset from a TEX/LATEX file prepared by the author.